IS-T-714

PROTON IRRADIATION OF VANADIUM

Paul John Hultgren

M. S. Thesis submitted to Iowa State University

Ames Laboratory, ERDA
Iowa State University
Ames, Iowa 50011

Date Transmitted: April 1976

PREPARED FOR THE U.S. ENERGY RESEARCH AND DEVELOPMENT ADMINISTRATION UNDER CONTRACT NO. W-7405-eng-82

DISCLAIMER

Available from: National Technical Information Service
U. S. Department of Commerce
P.O. Box 1553
Springfield, VA 22161

Price: Microfiche $2.25

Proton irradiation of vanadium

by

Paul John Hultgren

A Thesis Submitted to the
Graduate Faculty in Partial Fulfillment of
The Requirements for the Degree of
MASTER OF SCIENCE

Department: Materials Science and Engineering
Major: Metallurgy

Approved:

Tom E. Scott
In Charge of Major Work

For the Major Department

For the Graduate College

Iowa State University
Ames, Iowa

1976

TABLE OF CONTENTS

Proton irradiation of vanadium

by

Paul John Hultgren

ABSTRACT

Radiation blisters were produced on vanadium, niobium and molybdenum after bombardment with 150 Kev protons. The proton fluxes ranged from approximately $3(10^{15})$ to $3(10^{16})$ H^+/sec-sq cm while the proton fluence ranged from $8(10^{17})$ to $7(10^{19})$ H^+/sq cm. Increases in the proton fluence produced an increase in blister size and a decrease in the blister density. The formation of blisters at temperatures below the hydride dissociation temperature was demonstrated for vanadium.

I. INTRODUCTION

Deficiencies in knowledge concerning radiation effects on materials generates an economic impact estimated at $480 million in 1974, with an expected increase of over $1 billion by 1982 (1). The developmental programs for Controlled Thermonuclear Reactors (CTR) have focused considerable attention on the potential materials problems. An indication of the conceptual CTR design as presented by Fraas and Postma (2) (see Figs. 1 and 2) describes a vacuum vessel that will surround a magnetically confined plasma. Experience has shown that complete confinement using magnetic bottling techniques can not be expected, and as a result a portion of the plasma will escape and strike the "first wall" of the containment vessel.

Plasma particles with sufficient energy, move through the lattice of the "first wall" material displacing lattice atoms until the projectile particle is trapped within the lattice. The dissipation of the plasma projectile's energy within the lattice may result in severe damage to the bombarded lattice.

The damage generated by the bombardment of the "first wall" can result in the development of radiation blistered surfaces. These blisters threaten the success of the fusion reactor (CTR) by limiting the service life of the "first wall" due to the exfoliation of metal surfaces leading to a loss in mechanical integrity and by contaminating the plasma. Since current designs for the CTR promote use of a D-T fuel cycle,

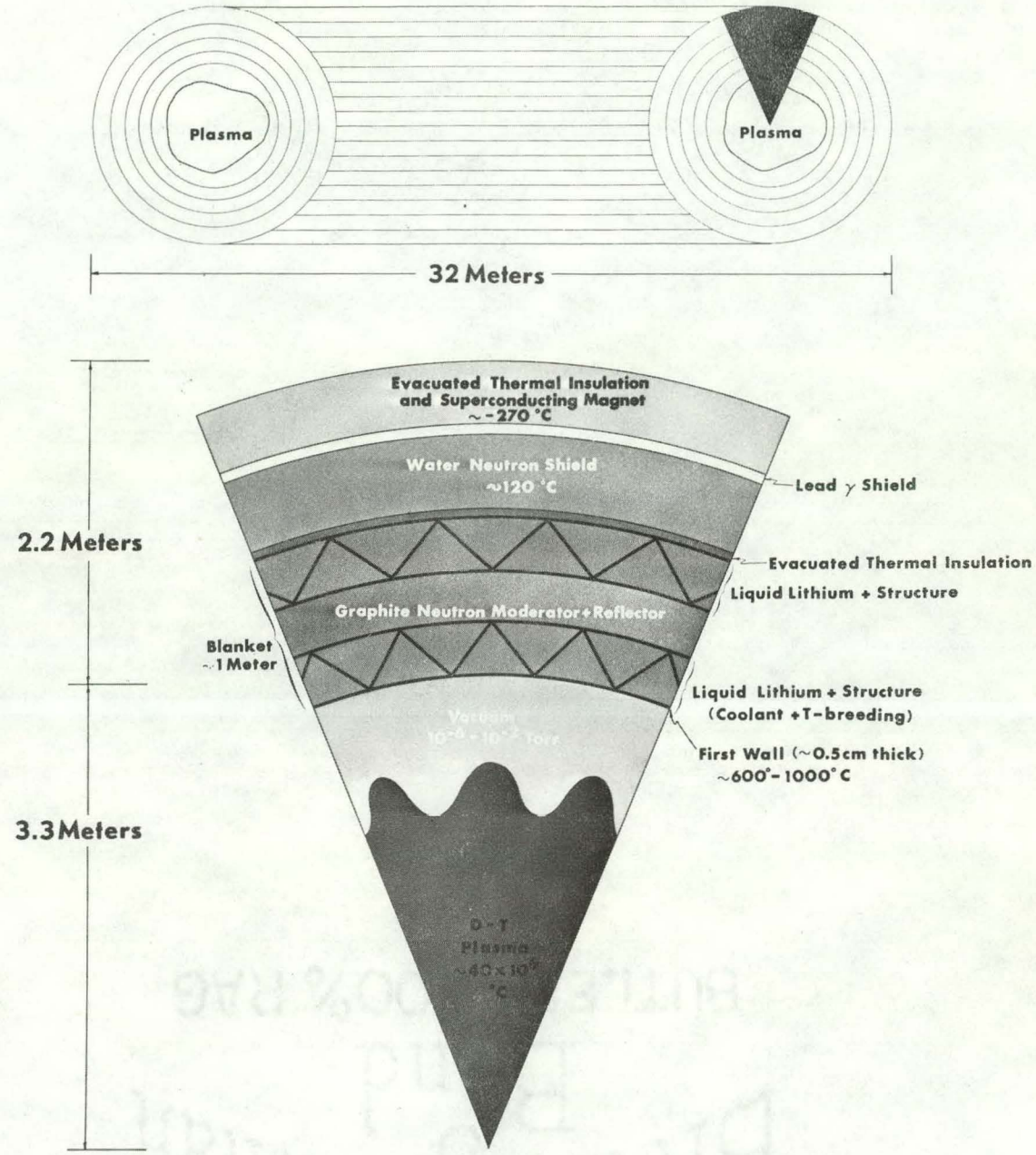

CROSS-SECTION OF A CONCEPTUAL CTR CORE DESIGN

Figure 1. A conceptual CTR core cross-section as presented by Fraas and Postma (2)

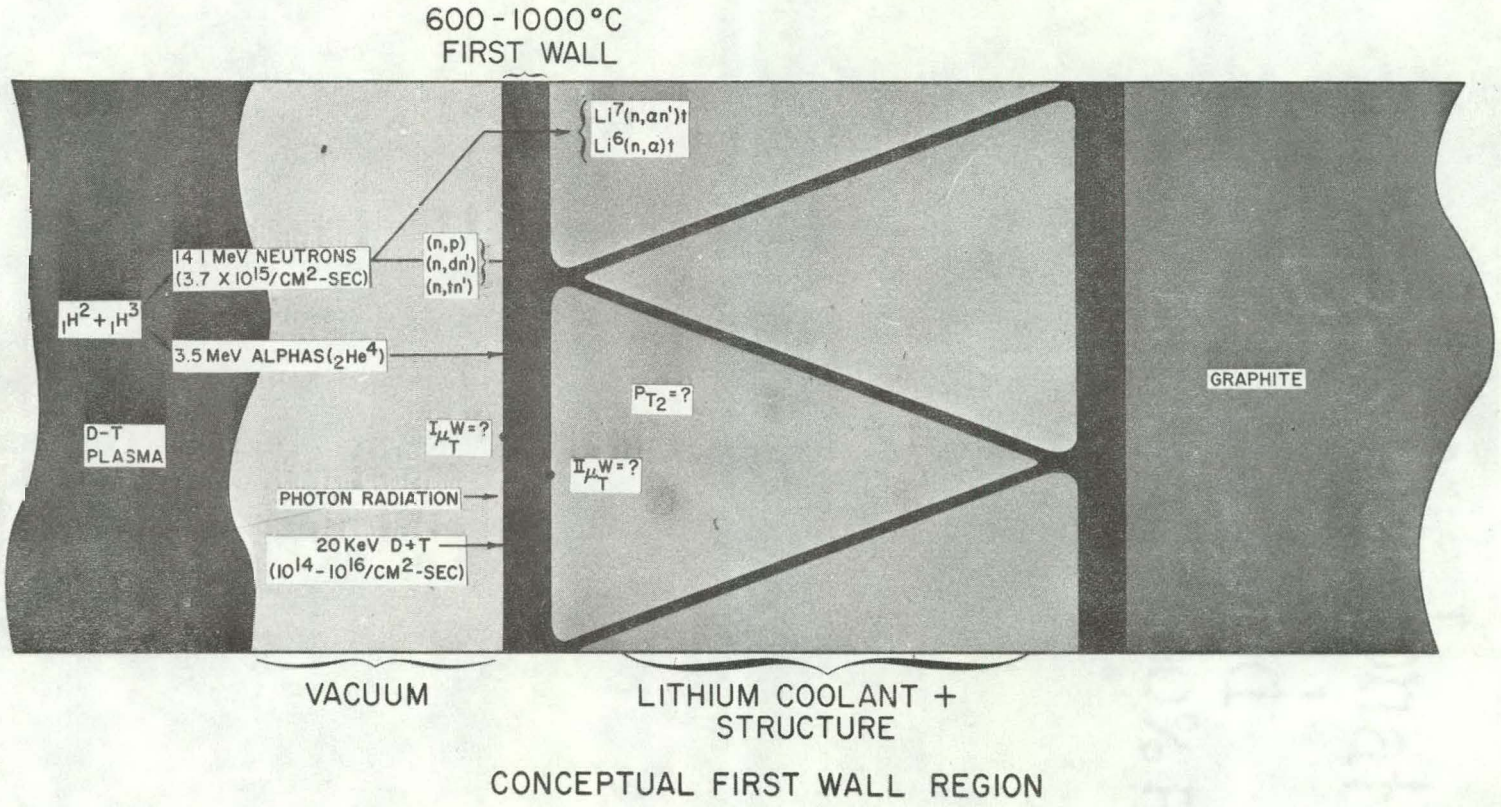

Figure 2. An enlarged view of the "first wall" region of the conceptual CTR core illustrated in Figure 1 indicating the anticipated environmental conditions

attention has been directed toward radiation damage generated from the bombardment of materials by hydrogen isotopes and helium.

The demands made upon the "first wall" of the CTR suggest the use of vanadium, niobium, molybdenum and their alloys because of their good neutronic character and mechanical properties at the projected CTR operating temperature of 600° to 1000°C (3). The projected particle current on the "first wall" due to neutral deutrium and tritium is estimated to be 10^{14} to 10^{16} particles/sec-sq cm with a energy of 20 Kev (3,4). This particle flux containing hydrogen isotopes is expected to deposit a high percentage of the ions within the material (3,4,5,6). These conditions will be contributing factors in the production of radiation blisters.

The occurrence of radiation blisters on vanadium and niobium has been well documented (7-14). Studies have examined blister shape, size and density as related to projectile energy, flux, fluence, target temperature, channeling conditions and initial defect concentration (8). Nevertheless, the conditions contributing to blister formation are not well defined, and low energy proton bombardment of refractory materials, such as vanadium, has not been investigated thoroughly.

The blistering phenomenon has been observed under a variety of circumstances which were not related to a radiation environment (15-18). The nature of blister formation by pro-

ton bombardment embraces characteristics akin to the nonequilibrium deposition of hydrogen associated with cathodic charging.

Radiation blistering is a localized bulging of a surface due to an increase in the internal gas pressure resulting from exposure to a radiation environment. This pressure increase is characteristic of the nonequilibrium deposition of gas atoms (e.g. hydrogen) in the metal matrix. The agglomeration of gas atoms typically occurs at lattice discontinuities such as grain boundaries, radiation induced void and second phase interfaces, resulting in the development of an equilibrium system between the gas, in molecular form, and the supersaturated matrix. In addition, hydrogen may react with impurities or alloying agents to form other gases, such as the formation of methane from reaction with a carbide. Molecular hydrogen or the gaseous reaction products have difficulty diffusing through the metal. The accumulation of gases can result in the development of gas pressures large enough to exceed the material's yield strength, resulting in local deformation. This deformation can appear as an internal fissure or, when the gas pocket is near the surface, a blister.

This research project was conceived and carried out in an attempt to provide qualitative information concerning the production of radiation blistered surfaces on pure vanadium metal using 150 Kev proton radiation. This project required the

modification of an existing accelerator installation to facilitate the irradiation of vanadium targets with protons in a controlled manner.

II. MATERIALS AND PROCEDURES

A. Sample Preparation

The vanadium metal used to fabricate targets for ion irradiation was prepared by the iodide refining process described by Carlson and Owen (19). The chemical analysis of the vanadium metal is indicated in Table 1. The analyses indicated in Table 1 were obtained using spectrochemical methods. The concentration of interstitial impurities was determined using vacuum fusion techniques for hydrogen, oxygen and nitrogen analyses, while carbon concentration was determined using the combustion method.

The material was cold rolled from the ingot to form a vanadium sheet 0.015 inch (0.038 cm) thick. The sheet was sheared into two inch squares, cleaned and then annealed in a vacuum of 10^{-8} torr (1.3×10^{-6} Pa) or better for two hours at 1000°C after which the furnace power was cut and the system was allowed to cool to room temperature while under vacuum. The squares of vanadium were then machined to the appropriate diameter (see Fig. 3a).

Development of a suitable sample surface was accomplished by electropolishing techniques. The electropolishing was preformed using a 25/75 by volume H_2SO_4/methanol solution at 0°C with an open circuit potential of 12 volts. In addition, one side of each sample was masked to provide for more effective polishing by reducing the surface area to be polished which

Table 1. Chemical analyses of materials (PPM by weight)

	Mo	Nb[a]	V	V[b]
Al	--	<20	<20	<100
B	--	<1	--	--
Ba	--	<50	--	<50
Ca	--	<20	<<39	<50
Cd	--	<5	--	<50
Co	--	<10	--	--
Cr	--	<20	150	<200
Cu	<200	<20	<25	<100
Fe	<100	<50	400	<500
Hf	--	<100	--	--
Mg	<200	<20	<15	<100
Mn	--	<20	<25	<50
Mo	Bal.	--	--	--
Nb	--	Bal.	--	--
Ni	--	<20	35	<400
Pb	--	<20	--	--
Si	--	<50	<40	<400
Sn	--	<20	--	--
Ta	--	560	--	--
Ti	--	<20	<25	--
V	--	<20	Bal.	Bal.
W	--	<100	--	--
Zr	--	< 50	--	<500
C	<5	10	100	--
O	45	31	364	--
N	--	27	88	--
H	--	<5	3	--

[a]Analysis by vendor.

[b]Target samples V-1 thru V-4 were fabricated using the electrolytically refined vanadium corresponding to analysis results in row 5; whereas, all other vanadium target samples were fabricated from the iodide refined vanadium corresponding to the analysis results in row 4.

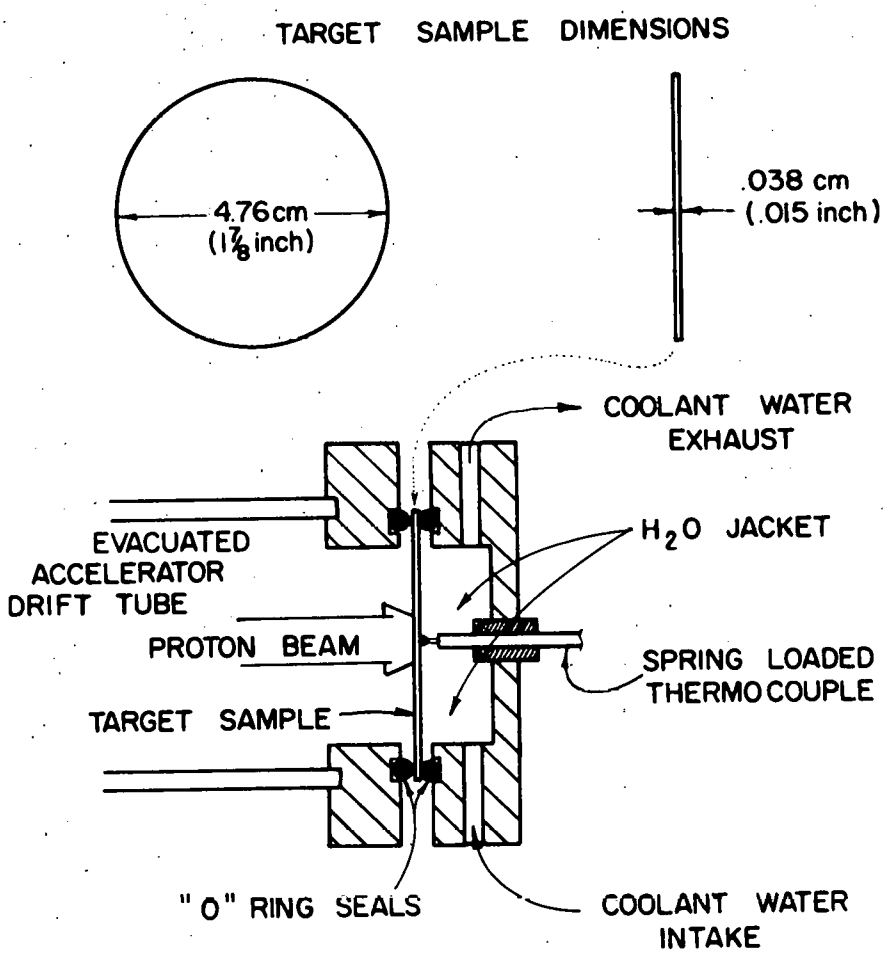

Figure 3a. Target sample dimensions and schematic representation of the sample position during irradiation

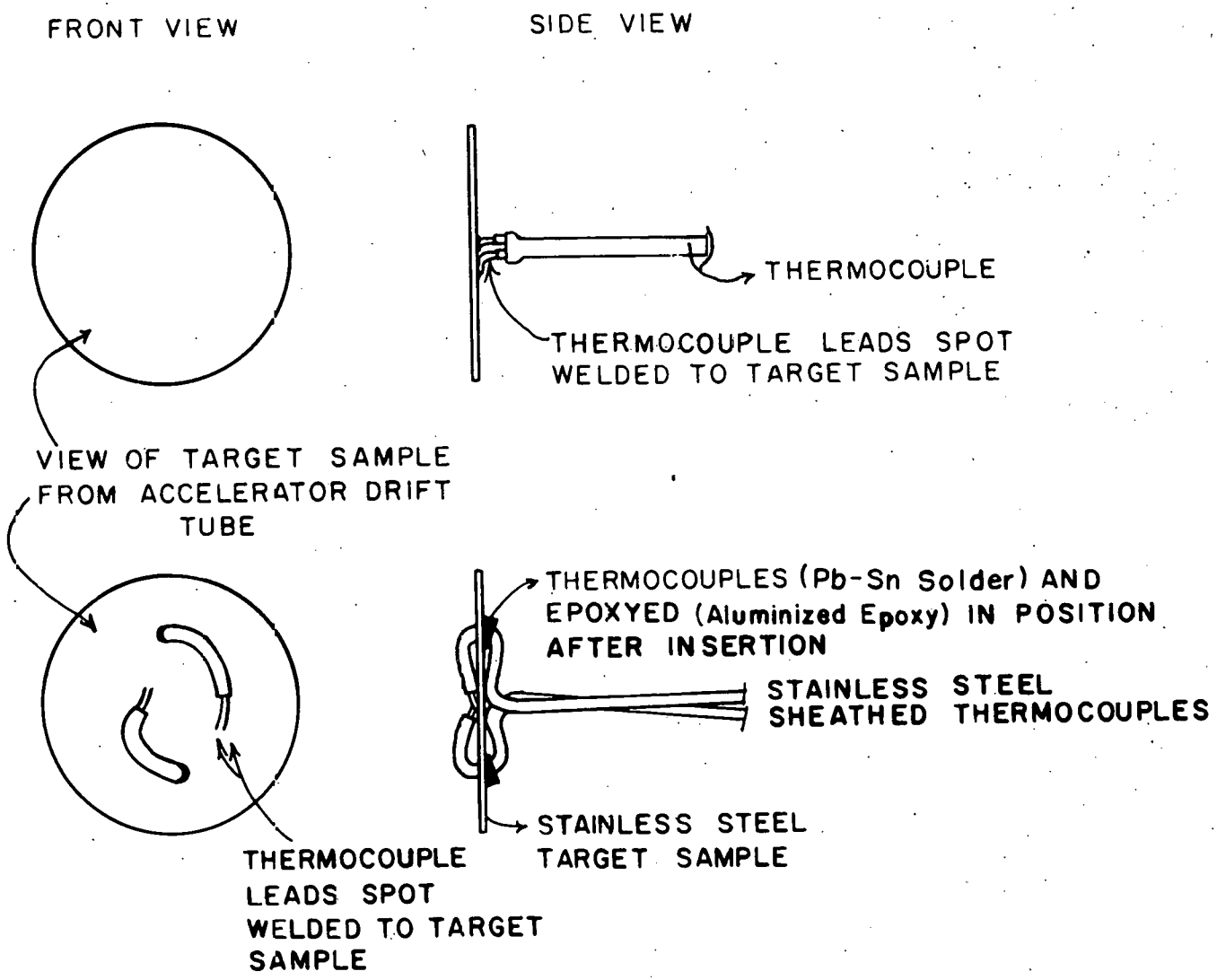

Figure 3b. Thermocouple positioning for temperature measurement during irradiation

reduces the current requirement during polishing.

Finally, the vanadium targets were annealed a second time to drive off excess hydrogen which may have been picked up during electropolishing and to insure a more uniform grain structure after machining. The samples were then stored in vacuum until needed.

Although, the major research emphasis dealt with proton bombardment of vanadium, a few samples of niobium and molybdenum were produced and irradiated. These materials were fabricated in a manner similar to the vanadium samples with a few expections.

The molybdenum samples were fabricated from commercially available 0.015 inch (0.038 cm) sheet. During electropolishing of molybdenum the electrolyte temperature was maintained between -45°C and -35°C while using an open circuit potential of 45 volts. The niobium samples were rolled from a 0.25 inch (0.64 cm) plate to 0.015 inch (0.038 cm), and all annealing stages were carried out at 1150°C. The niobium samples were chemically polished in place of electropolishing, using a 20/20/10/50 by volume solution of HNO_3, H_2SO_4, HF and methanol.

B. Proton Beam Source

The radiation environment was provided by a modified Texas Nuclear Cockroft-Walton Linear Accelerator neutron generation system. In normal operation the "generator" would accelerate D^+ particles into a tritium doped target to produce 14.7

Mev neutrons typically used for activation studies. In order to study the effects of proton radiation, the deuterium gas was replaced with hydrogen and the tritiated target was replaced with one of the vanadium targets described previously. The vanadium target samples were positioned such that the sample's electropolished surface would be subject to the projectile ion flux. The target was cooled by water flow through the accelerator end cap, and the target and "O"-rings formed a vacuum seal for the accelerator drift tube and a water seal for the coolant in the end cap. In addition, the accelerator end cap was modified to accommodate placement of a thermocouple (see Figs. 3a and 3b).

After the target was positioned, the accelerator drift tube was evacuated to 10^{-6} torr (1.3×10^{-4} Pa) or better. During operation the maximum beam current available was 1 ma and the maximum accelerating potential was 150 Kev. The duration of a single irradiation was limited by the accelerator vacuum system due to the gradual heating of the system's ion pump. Typical beam times available for a single radiation exposure were 35 to 50 minutes. However, multiple exposures were possible by judicious duplication of accelerator focus, extraction and palladium leak settings.

Accelerator parameters monitored and regulated during irradiation were:

Beam Energy - Acceleration potential for the projectile ion (i.e. proton).

Beam Current - The number of projectile ions striking the target per second.

Beam Diameter - The diameter of the column of projectile ions containing the major portion of the stream of accelerated ions.

Beam Position - The location of the projectile column on the target

Beam Time - The total time during which ions are allowed bombard the sample surface (i.e. target).

Ion Flux - The number of projectile ions striking the target per second per square centimeter.

Ion Fluence - The total number of projectile ions that have struck the target per square centimeter (i.e. dose).

Temperature - The temperature of the sample was monitored. Regulation of the temperature was a function of the other parameters indicated above, and therefore, was not subject to direct regulation.

C. Experimental Procedure

Once the target was in position and a suitable vacuum was obtained, accelerator controls were preset to minimize adjustment during the actual bombardment. The beam current, beam position and beam diameter required adjustment while bombardment was in progress. However, the transient period, during

which these parameters were stabilized, was less than 5% of the total beam time.

The beam position and the beam diameter were monitored and initially selected visually. Since visual observation required personnel entry into the accelerator room during operation, the room was carefully monitored for the presence of various harmful forms of radiation. The proton beam appeared as a column of blue light which shown all along the accelerator drift tube, and provided a distinct position indication on the target. Because the beam diameter was initially selected visually, the reproducibility of that selection was checked using the accelerator focus setting. Later, the diameter was checked for correlation to the blister area observed after microscopic examination of each irradiated target. When a sample was removed from the accelerator, the sample was monitored. The monitoring was a safety precaution used to avoid the spread of tritium which was present in the accelerator as residue from neutron generation work.

The investigation of the vanadium target samples was accomplished using optical microscopy and scanning electron microscopy (S.E.M.) techniques. All microscopy was performed on the as-irradiated surface with no additional preparation other than a light alcohol or acetone rinse. The S.E.M. studies were accomplished using a Cambridge S-4 Stereoscan electron microscope which could reproducibly resolve at least 200 Å. Analysis of the photomicrographs was made using a

Carl-Zeiss particle analyzer.

Sample surfaces were surveyed at low magnification using an optical microscope to determine the extent of the blistered area for correlation to the apparent beam diameter and shape during bombardment. Figs. 4 through 6 show examples of blistered regions using optical microscopy.

S.E.M. photographs of the blistered surfaces were used to obtain blister size and density information. In addition, the S.E.M.'s goniometric stage made possible the development of a systematic survey pattern. The pattern was used to provide an indication of the variation in the blister character across the damaged surface. The S.E.M. photomicrographs presented in Figs. 7 through 12b are typical of the photographs which were used to investigate the nature of the radiation blisters.

Three methods of measuring the sample temperature were employed. These methods all used thermocouples as temperature sensors. However, the thermocouple configuration was varied as indicated in Figs. 3a and 3b, to provide more accurate denotation of the sample temperature during irradiation.

Sample V7 was prepared to provide a cross section of the blistered region for hydride content investigation using cold stage optical microscopy. The hydride investigation was conducted using the techniques and apparatus described by Sherman, Owen and Scott (20) for determination of hydride transformation temperature.

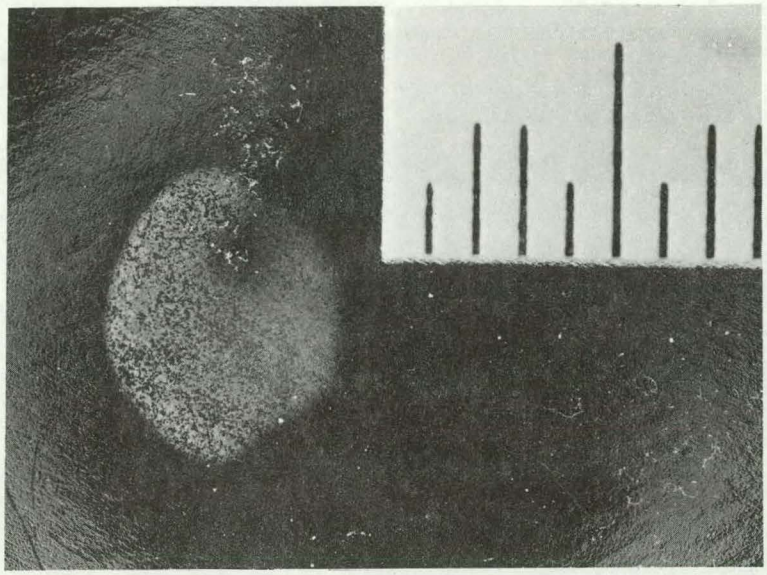

Beam spot at low magnification (each scale division represents 1 mm)

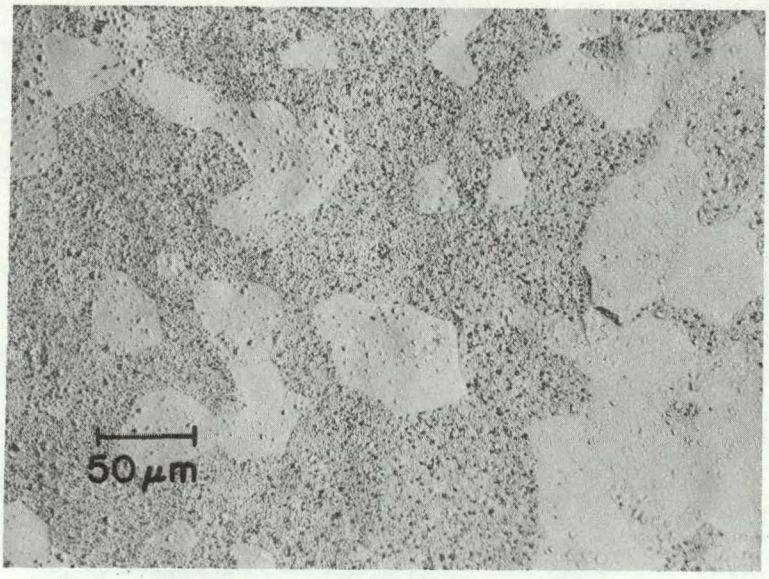

Blistered region at moderate magnification

Figure 4. Optical microscopy for sample number V8 - annealed sample irradiated with 1 ma beam current

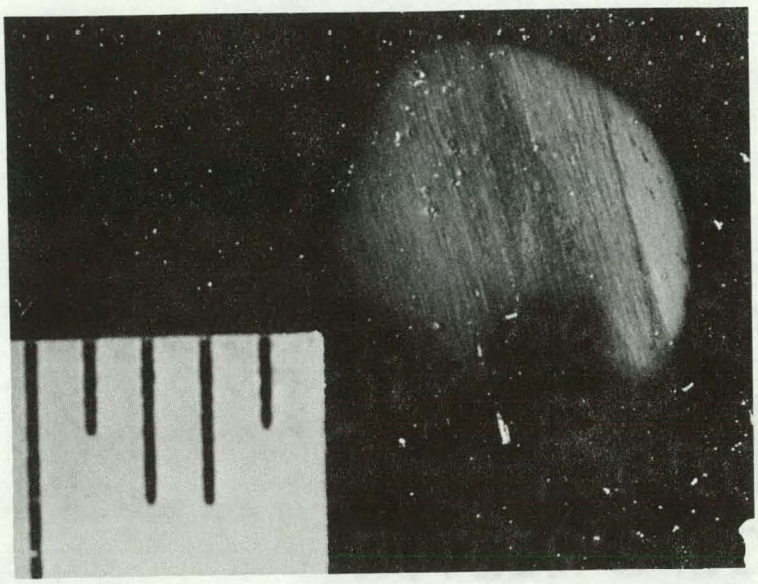

Beam spot at low magnification (each scale division represents 1 mm)

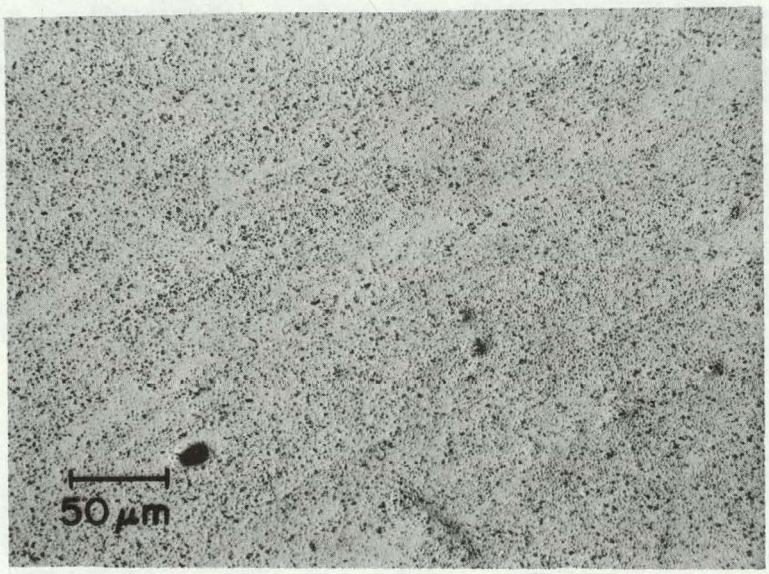

Blistered region at moderate magnification

Figure 5. Optical microscopy for sample number V10 - cold worked sample irradiated with 1 ma beam current

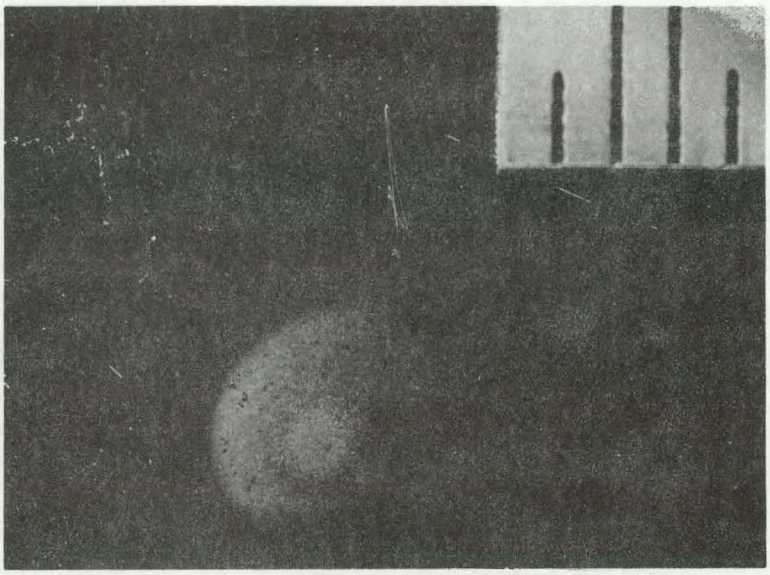

Beam spot at low magnification (each scale division represents 1 mm)

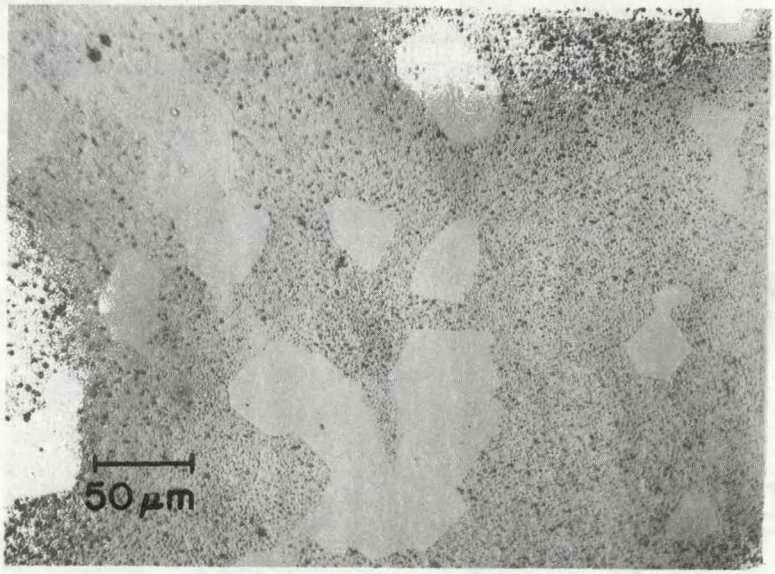

Blistered region at moderate magnification

Figure 6. Optical microscopy for sample number V12 - annealed sample irradiated with 0.1 ma beam current

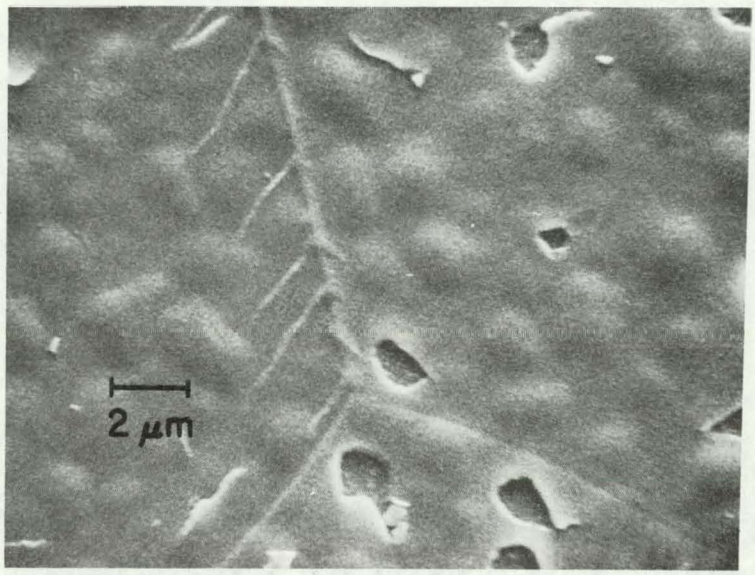

Sample V6
photomicrograph
number 9

Region: center

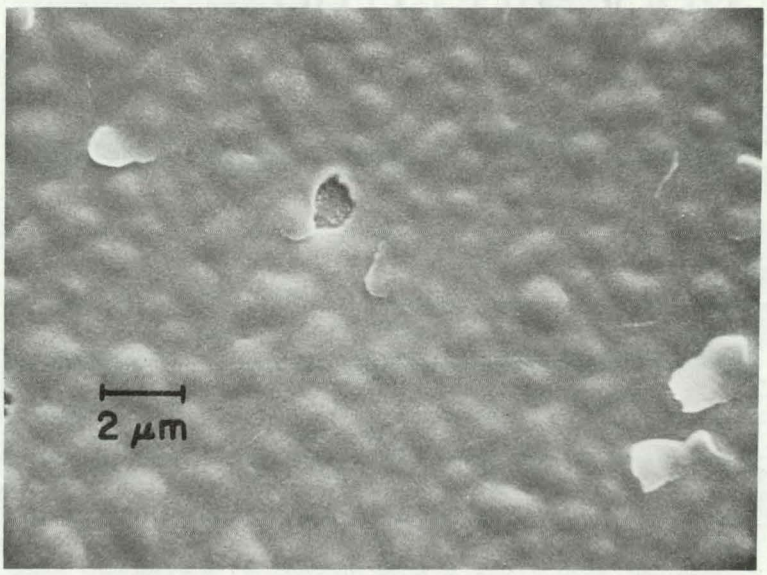

Sample V7
photomicrograph
number 9

Region: edge

Figure 7. S.E.M. photographs depicting a portion of the blistered regions of samples V6 and V7

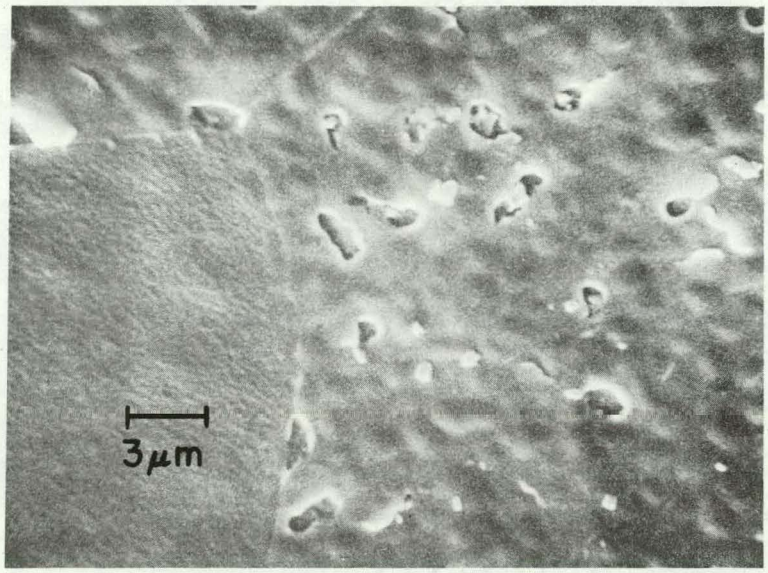

Sample V8
photomicrograph
number 9

Region: center

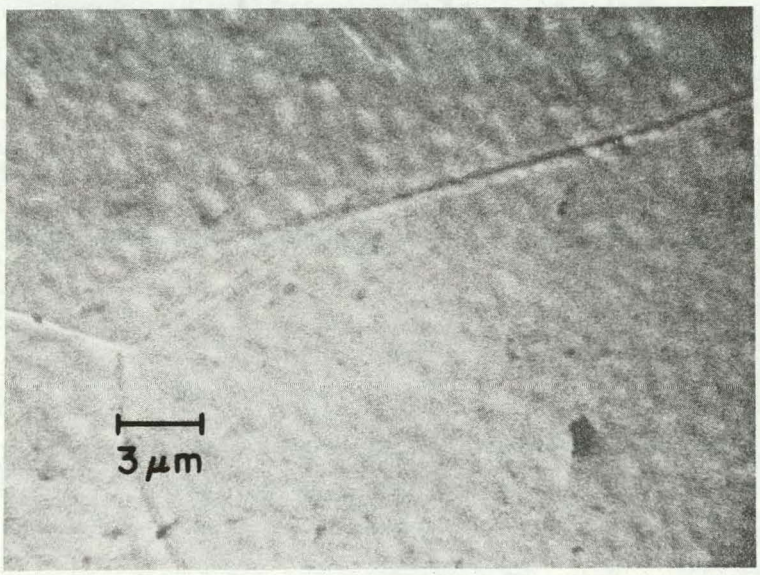

Sample V9
photomicrograph
number 1

Region: intermediate

Figure 8. S.E.M. photographs depicting a portion of the blistered regions of samples V8 and V9

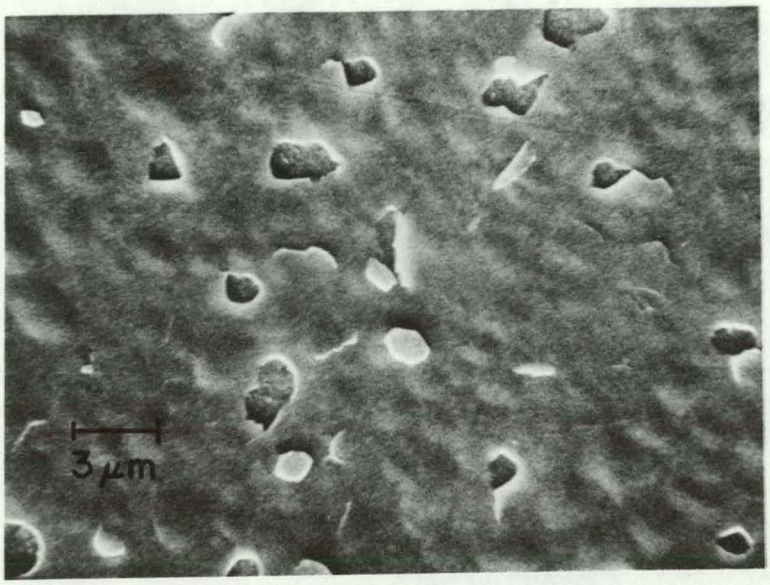

Sample V10
photomicrograph
number 4

Region: intermediate

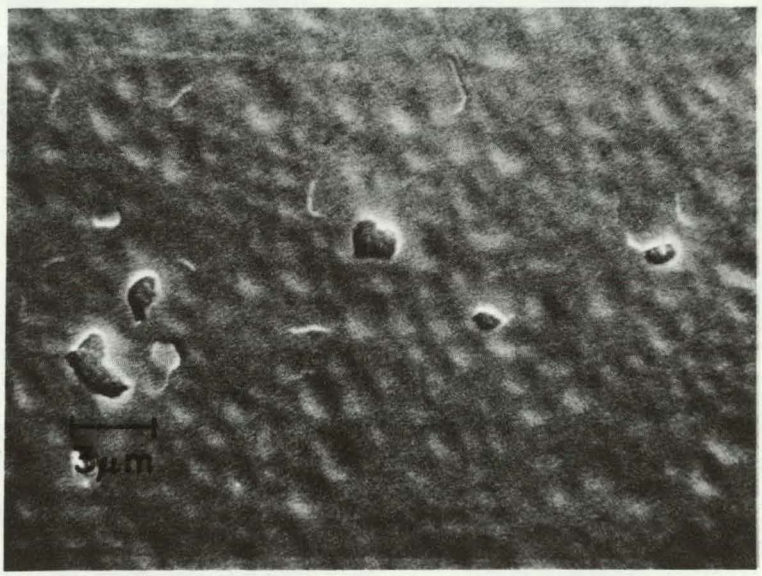

Sample V11
photomicrograph
number 2

Region: intermediate

Figure 9. S.E.M. photographs depicting a portion of the blistered regions of samples V10 and V11

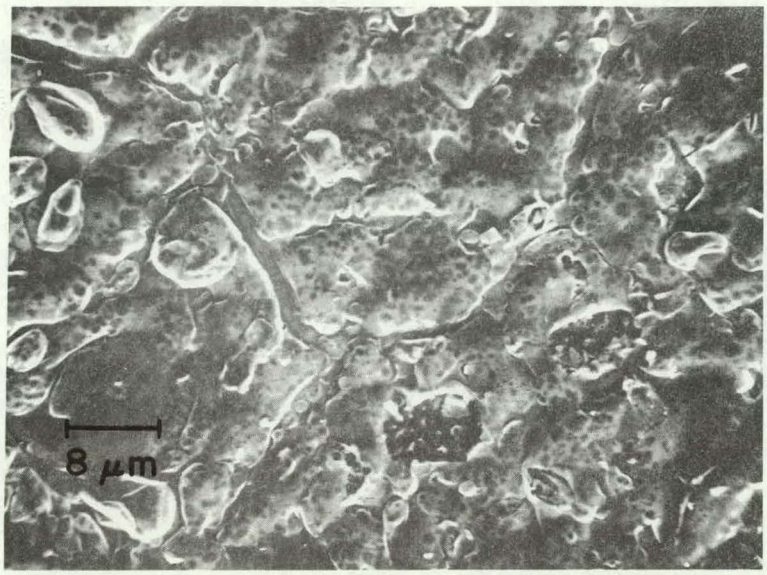

Sample V12
photomicrograph
number 3

Region: center

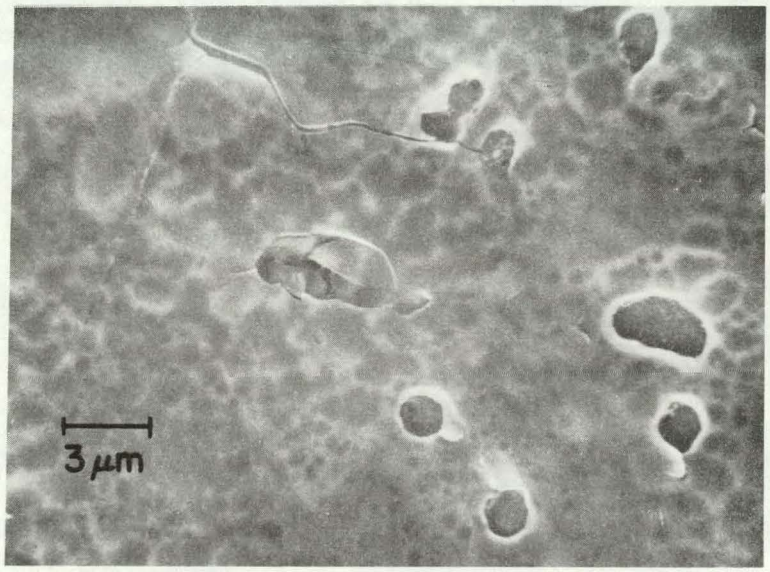

Sample V12
photomicrograph
number 4

Region: center

Figure 10a. S.E.M. photograph sequence for sample V12 with beam spot regions indicated

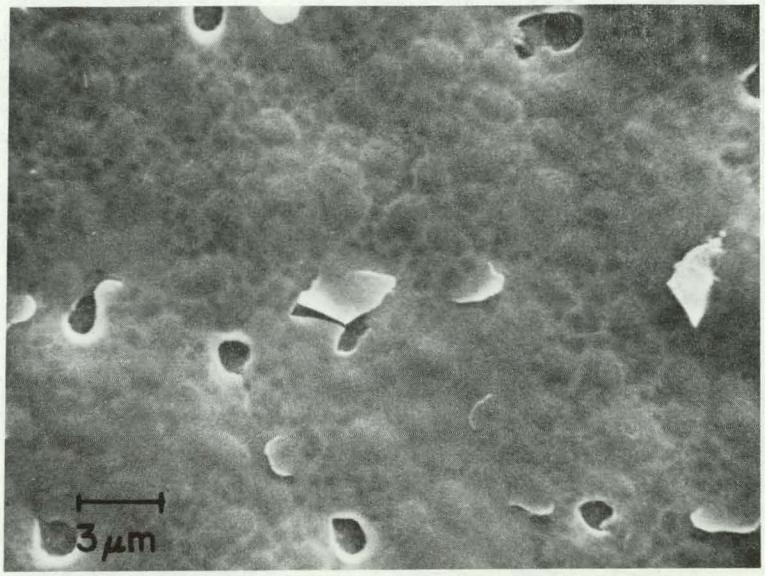

Sample V12
photomicrograph
number 5

Region: intermediate

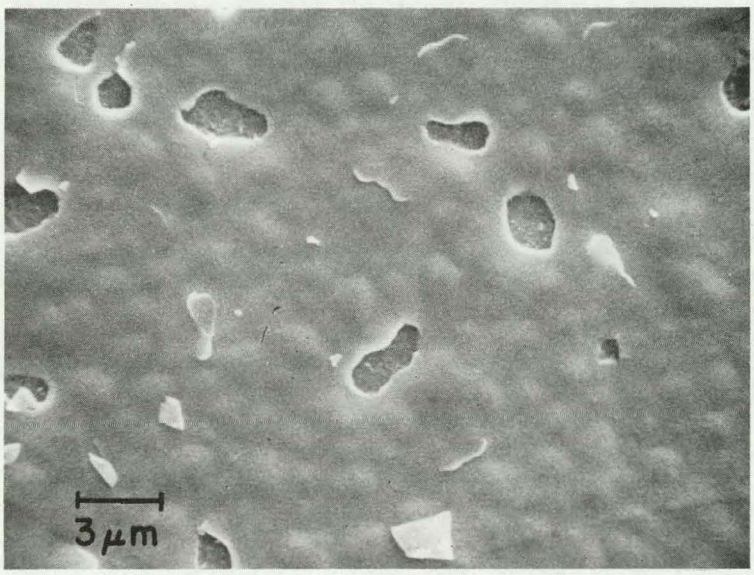

Sample V12
photomicrograph
number 6

Region: intermediate

Figure 10b. S.E.M. photograph sequence for sample V12 with beam spot regions indicated

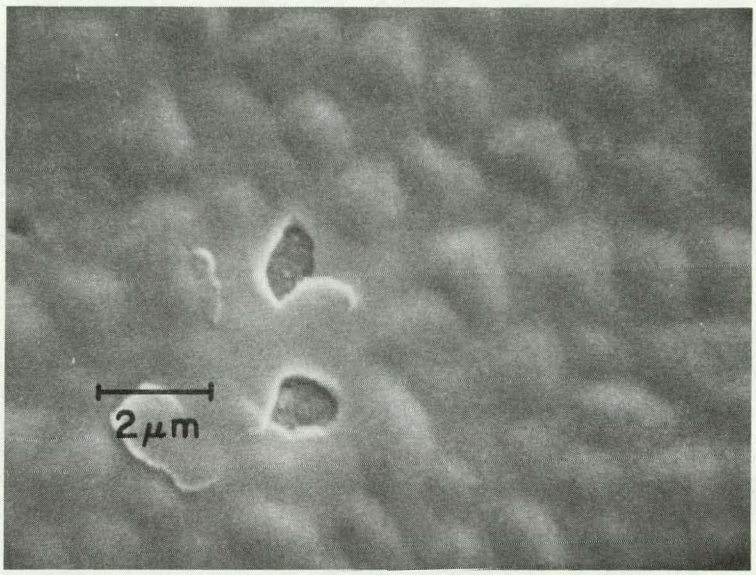

Sample V12
photomicrograph
number 2

Region: edge

Figure 10c. S.E.M. photograph sequence for sample V12 with beam spot region indicated

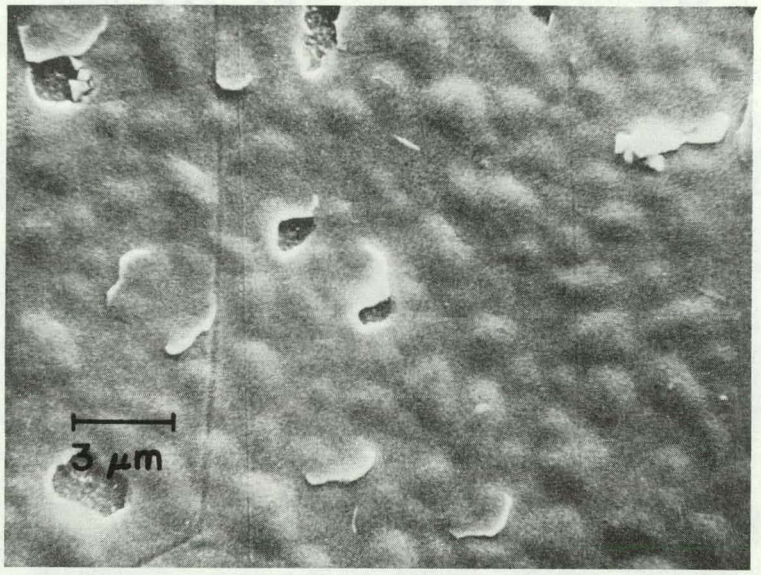

Sample V13
photomicrograph
number 3

Region: intermediate

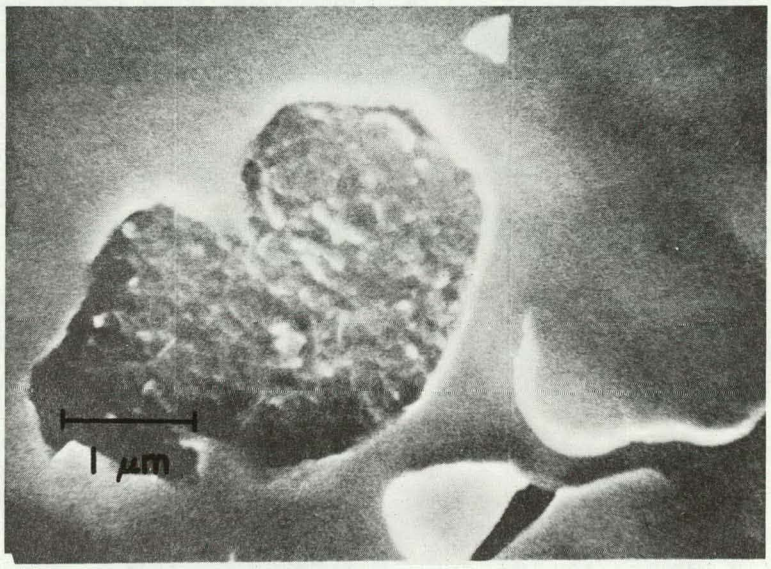

Sample V13
photomicrograph
number 6

Region: center

Figure 11. S.E.M. photographs depicting a portion of the blistered regions for sample V13

Sample Nb-1
photomicrograph
number 1

Region: center

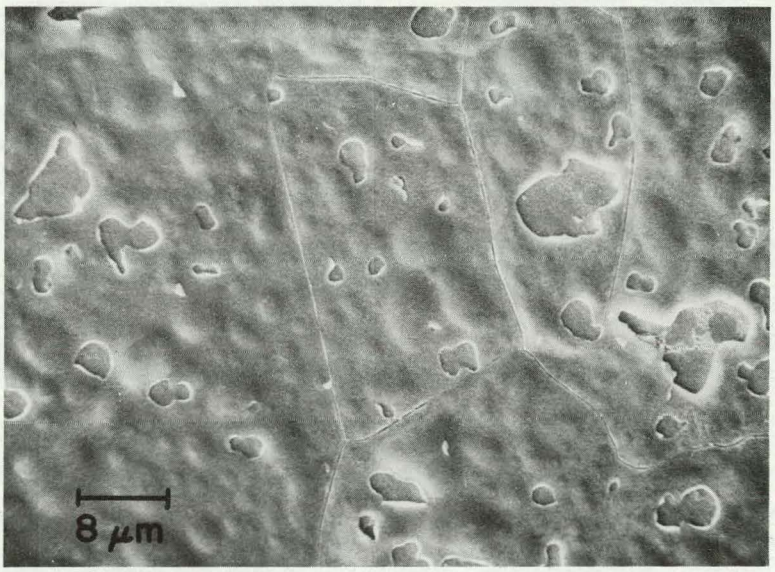

Sample Nb-1
photomicrograph
number 2

Region: intermediate

Figure 12a. S.E.M. photographs depicting a portion of the blistered regions of sample Nb-1

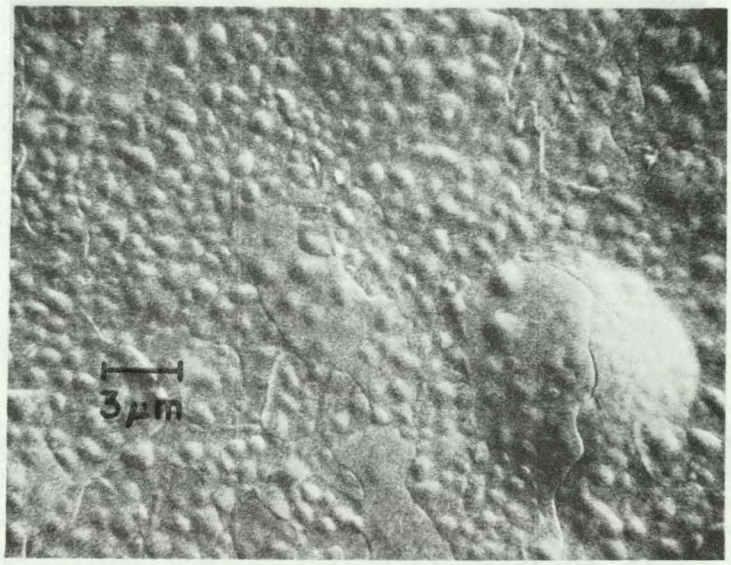

Sample Mo-2
photomicrograph
number 3

Region: edge

Figure 12b. S.E.M. photograph depicting a portion of the blistered region of sample Mo-2

The analyses given in Table 1 were supplemented by additional analysis work performed on each individual sample target. Since there was little or no opportunity for substitutional contamination of the sample material during experimentation, interstitial analyses were performed for hydrogen, oxygen, nitrogen and carbon. Vacuum fusion techniques were used to develop gas analysis information on two areas of each sample representing an unirradiated portion and an irradiated portion of the samples. Carbon analyses were performed on an unirradiated portion of each sample using combustion techniques. The results of these analyses are presented in Appendix B.

D. Blister Measurements

Raw measurements of blister diameters apparent in each of the S.E.M. photographs are indicated in Appendix A, Tables A1 through A25. These measurements were converted to actual diameter values by dividing the measured diameter by the photograph magnification. The blister density was obtained by dividing the total number of blisters apparent in a photomicrograph by the photomicrograph area and multiplying by the photomicrograph magnification.

$$\text{Actual blister diameter} = \text{Measured diameter/photo magnification}$$

$$\text{Blister density} = \frac{\text{Number of blisters} \times \text{photo magnification}}{\text{Photo area}}$$

The results of the S.E.M. investigations were organized into three groups for each sample corresponding to the formation of

three beam spot regions related to the division of the beam spot radius into three equal segments. These groups were used to describe the variation of the blister character at different positions in the beam spot. These regions were designated as "center", "intermediate" and "edge".

After the data were converted to actual blister diameter values, two methods were used to investigate the blister diameter data. Compilation of the diameter values was made by taking the arithmetic mean of the diameter values for each photomicrograph and by developing a blister size distribution curve for each photomicrograph. The data presented in Table 2 were developed by the determination of the arithmetic mean of the blister diameter values. Figs. A1 through A8 are representative of the distribution curves used to develop the data presented in Table 3. Table 4 indicates the blister size information for each sample overall and as related to each of the three beam spot regions. The blister density information for each photomicrograph is presented in Tables 5 and 6. Blister diameter values ranged from 1.9 μm to 1.2 μm, while blister density values ranged from 4.8 (10^3) to 11.3 (10^3) blisters/sq cm.

E. Temperature Measurement

Measurement of the sample temperature during bombardment proved to be a complicated task. Initially, each sample's temperature was measured using a spring loaded thermocouple

Table 2. Mean blister diameter values for each photomicrograph with beam spot region indicated

Sample number	Calculated mean blister diameters (μm)								
	Photo 1	Photo 2	Photo 3	Photo 4	Photo 5	Photo 6	Photo 7	Photo 8	Ave.
V6 Center	1.93	1.71	----	----	----	2.17	----	----	1.94
V6 Intermediate	----	----	----	----	----	----	1.73	----	1.73
V6 Edge	----	----	----	1.69	1.26	----	----	----	1.48
V7 Center	----[a]	1.65	----	----	----	----	----	----	1.65
V7 Intermediate	----[a]	----	1.82	----	----	1.69	----	----	1.76
V7 Edge	----[a]	----	----	1.36	1.49	----	1.25	1.52	1.41
V8 Center	1.74	1.79	----	----	----	1.50	----	----	1.68
V8 Intermediate	----	----	1.30	----	----	----	1.83	----	1.57
V8 Edge	----	----	----	1.36	1.33	----	----	----	1.35
V9 Center	----	----	----	----	----	----	----	----	----
V9 Intermediate	1.07	1.13	1.28	----	----	----	----	----	1.16
V9 Edge	----	----	----	----	----	----	----	----	----
V10 Center	----	1.55	1.48	----	----	----	2.22	----	1.75
V10 Intermediate	----	----	----	1.47	----	----	----	1.91	1.64
V10 Edge	----	----	----	----	1.37	1.10	----	----	1.23
V11 Center	----	----	----	----	----	----	----	----	----
V11 Intermediate	1.11	1.15	1.34	----	----	----	----	----	1.20
V11 Edge	----	----	----	----	----	----	----	----	----
V12 Center	----	----	----[a]	----[a]	----	----	----	----[a]	----
V12 Intermediate	----	----	----[a]	----[a]	1.31	1.57	----	----[a]	1.44
V12 Edge	----	1.34	----[a]	----[a]	----	----	1.24	----[a]	1.29
V13 Center	1.43	----	----	----	1.40	----	----	----	1.42
V13 Intermediate	----	----	1.46	----	----	----	1.42	----	1.44
V13 Edge	----	----	----	1.18	----	----	----	1.29	1.24

[a]Central region blistered severely.

Table 3. Blister diameter values determined from distribution plots for each photomicrograph with beam spot region indicated

Sample number	Graphically determined blister diameters (μm)								
	Photo 1	Photo 2	Photo 3	Photo 4	Photo 5	Photo 6	Photo 7	Photo 8	Ave.
V6 Center	1.7	1.6	---	---	---	1.9	---	---	1.8
V6 Intermediate	---	---	---	---	---	---	1.6	---	1.6
V6 Edge	---	---	---	1.7	1.1	---	---	---	1.4
V7 Center	---[a]	1.4	---	---	---	---	---	---	1.4
V7 Intermediate	---[a]	---	1.8	---	---	1.7	---	---	1.8
V7 Edge	---[a]	---	---	1.4	1.5	---	1.3	1.5	1.4
V8 Center	1.7	1.7	---	---	---	1.4	---	---	1.6
V8 Intermediate	---	---	1.3	---	---	---	1.5	---	1.4
V8 Edge	---	---	---	1.3	1.4	---	---	---	1.4
V9 Center	---	---	---	---	---	---	---	---	---
V9 Intermediate	1.1	1.2	1.3	---	---	---	---	---	1.2
V9 Edge	---	---	---	---	---	---	---	---	---
V10 Center	---	1.6	1.5	---	---	---	1.4	---	1.5
V10 Intermediate	---	---	---	1.4	---	---	---	1.7	1.6
V10 Edge	---	---	---	---	1.4	1.1	---	---	1.3
V11 Center	---	---	---	---	---	---	---	---	---
V11 Intermediate	1.1	1.1	1.4	---	---	---	---	---	1.2
V11 Edge	---	---	---	---	---	---	---	---	---
V12 Center	---	---	---[a]	---[a]	---	---	---	---[a]	---
V12 Intermediate	---	---	---[a]	---[a]	1.2	1.5	---	---[a]	1.4
V12 Edge	---	1.4	---[a]	---[a]	---	---	1.1	---[a]	1.3
V13 Center	1.2	---	---	---	1.2	---	---	---	1.2
V13 Intermediate	---	---	1.3	---	---	---	1.3	---	1.3
V13 Edge	---	---	---	1.2	---	---	---	1.2	1.2

[a]Central region blistered severely.

Table 4. Summary of the blister size information presented in Tables 4 and 5 as related to the bombardment parameters of ion flux and fluence

Sample number	Ion flux (10^{16})	Ion fluence[a] (10^{19})	Average blister diameter (μm) (points determined using arithmetic mean) Center	Interm.	Edge	Ave.	Average blister diameter (μm) (points as estimated from plot) Center	Interm.	Edge	Ave.
V-6	3.2	7.3	1.94	1.73	1.48	1.72	1.8	1.6	1.4	1.6
V-7	"	6.1	1.65	1.76	1.41	1.61	1.4	1.8	1.4	1.5
V-8	"	4.9	1.68	1.57	1.35	1.53	1.6	1.4	1.4	1.5
V-9	"	3.7	----	1.16	----	1.16	---	1.2	----	1.2
V-10	2.7	5.2	1.75	1.64	1.23	1.54	1.5	1.6	1.3	1.5
V-11	3.2	4.2	----	1.20	----	1.20	---	1.2	----	1.2
V-12	3.2	5.4	----	1.44	1.29	1.37	---	1.4	1.3	1.4
V-13	3.2	2.5	1.42	1.44	1.24	1.37	1.2	1.3	1.2	1.2

[a]The ion fluence indicated corresponds to the estimated ion fluence indicated in Table 2.

Table 5. Mean blister density values for each photomicrograph with beam spot region indicated

Sample number	Mean blister density [blisters per square centimeter x10^3]								
	Photo 1	Photo 2	Photo 3	Photo 4	Photo 5	Photo 6	Photo 7	Photo 8	Ave.
V6 Center	4.87	5.47	----	----	----	4.56	----	----	4.97
V6 Intermediate	----	----	----	----	----	----	5.32	----	5.32
V6 Edge	----	----	----	6.37	----	----	----	----	6.37
V7 Center	----[a]	5.15	----	----	----	----	----	----	5.15
V7 Intermediate	----[a]	----	5.05	----	----	4.50	----	----	4.78
V7 Edge	----[a]	----	----	6.09	7.13	----	8.76	----	7.33
V8 Center	5.83	5.54	----	----	----	5.98	----	----	5.78
V8 Intermediate	----	----	7.57	----	----	----	6.75	----	7.16
V8 Edge	----	----	----	7.66	7.91	----	----	----	7.79
V9 Center	----	----	----	----	----	----	----	----	----
V9 Intermediate	14.87	8.30	11.35	----	----	----	----	----	11.51
V9 Edge	----	----	----	----	----	----	----	----	----
V10 Center	----	6.04	7.43	----	----	----	4.16	----	5.88
V10 Intermediate	----	----	----	6.68	----	----	----	4.60	5.64
V10 Edge	----	----	----	----	8.71	13.86	----	----	11.29
V11 Center	----	----	----	----	----	----	----	----	----
V11 Intermediate	8.91	11.16	10.04	----	----	----	----	----	10.04
V11 Edge	----	----	----	----	----	----	----	----	----
V12 Center	----	----	----[a]	----[a]	----	----	----	----[a]	----
V12 Intermediate	----	----	----[a]	----[a]	13.14	8.01	----	----[a]	10.58
V12 Edge	----	6.06	----[a]	----[a]	----	----	6.74	----[a]	6.40
V13 Center	8.40	----	----	----	8.74	----	----	----	8.57
V13 Intermediate	----	----	8.07	----	----	----	7.06	----	7.57
V13 Edge	----	----	----	11.88	----	----	----	9.30	10.54

[a]Central region blistered severely.

Table 6. Summary of blister density information presented in Table 7 as related to the bombardment parameters of ion flux and fluence

Sample number	Ion flux (10^{16})	Ion fluence[a] (10^{19})	Average blister density (blisters per square centimeter x 10^3) Center	Intermed.	Edge	Average
V-6	3.2	7.3	4.97	5.32	6.37	5.55
V-7	"	6.1	5.15	4.78	7.33	5.75
V-8	"	4.9	5.78	7.16	7.79	6.91
V-9	"	3.7	----	11.51	----	11.51
V-10	2.7	5.2	5.88	5.64	11.29	7.60
V-11	2.7	4.2	----	10.04	----	10.04
V-12	3.2	5.4	----	10.58	6.40	8.49
V-13	3.2	2.5	8.57	7.57	10.54	8.91

[a]The ion fluence indicated corresponds to the estimated ion fluence indicated in Table 2.

on the side opposite the beam (see Fig. 3a). This method provided consistent temperature readings of 41°C to 44°C for an ion flux of approximately $3(10^{16})$ ions/sec-sq cm. However, these measurements were made on the water cooled side of the target sample, and the actual temperature of the target material was not indicated due to the flow of coolant around the thermocouple bead.

In order to minimize the effects of the coolant flow, the thermocouple design was altered to allow each thermocouple lead to be individually spot welded to the vanadium sample with approximately 0.13 inch (0.32 cm) separation (see Fig. 3b). This temperature measurement configuration yielded higher temperature values compared to the method indicated above. Finally, a method was devised to allow temperature measurement of the sample's beam side using direct thermocouple placement. This method used a stainless steel target with stainless steel sheathed thermocouples inserted into the evacuated accelerator drift tube through holes in the sample target. The thermocouples were soldered in position, and the solder joints were sealed with aluminized epoxy. These thermocouple leads were individually spot welded to the beam side of the stainless steel sample target as indicated in Fig. 3b. Both temperature measurement configurations, indicated in Fig. 3b, were used to provide information regarding the variation of sample temperature with changes in the proton flux. Table 7 contains the temperature data illustrated in Fig. 13 which

Table 7. Temperature measurements[a] of target sample during irradiation

Beam current (ma)	Beam diameter (cm)	Ion flux[b] ($x10^{16}$) (ions/sec-cm^2)	Temperature measured Beam side (°C)	Water side (°C)
0.10	1.0	0.2	--	39
0.25	1.1	0.3	--	56
0.30	1.6	0.2	46	--
0.40	1.6	0.3	47	--
0.42	1.3	0.4	58	--
0.50	1.3	0.5	60	--
0.60	1.6	0.4	55	--
0.60	0.8	1.6	--	78
0.64	"	1.7	61	--
0.65	"	1.8	69	--
0.66	"	1.8	68	--
0.70	"	1.9	61	--
0.80	"	2.2	71	--
0.83	"	2.3	81	--
0.85	"	2.3	86	--
0.86	"	2.4	84	--
0.87	"	2.4	92	--
1.00	0.9	2.3	--	121
1.00	0.8	2.7	--	102
1.00	0.8	2.7	--	82

[a]Measurements were made using the spot welded thermocouple configurations indicated in Figure 3b.

[b]Estimated ion flux determined by taking 85% of the calculated ion flux found using information in columns 1 and 2. See footnote on Table 8.

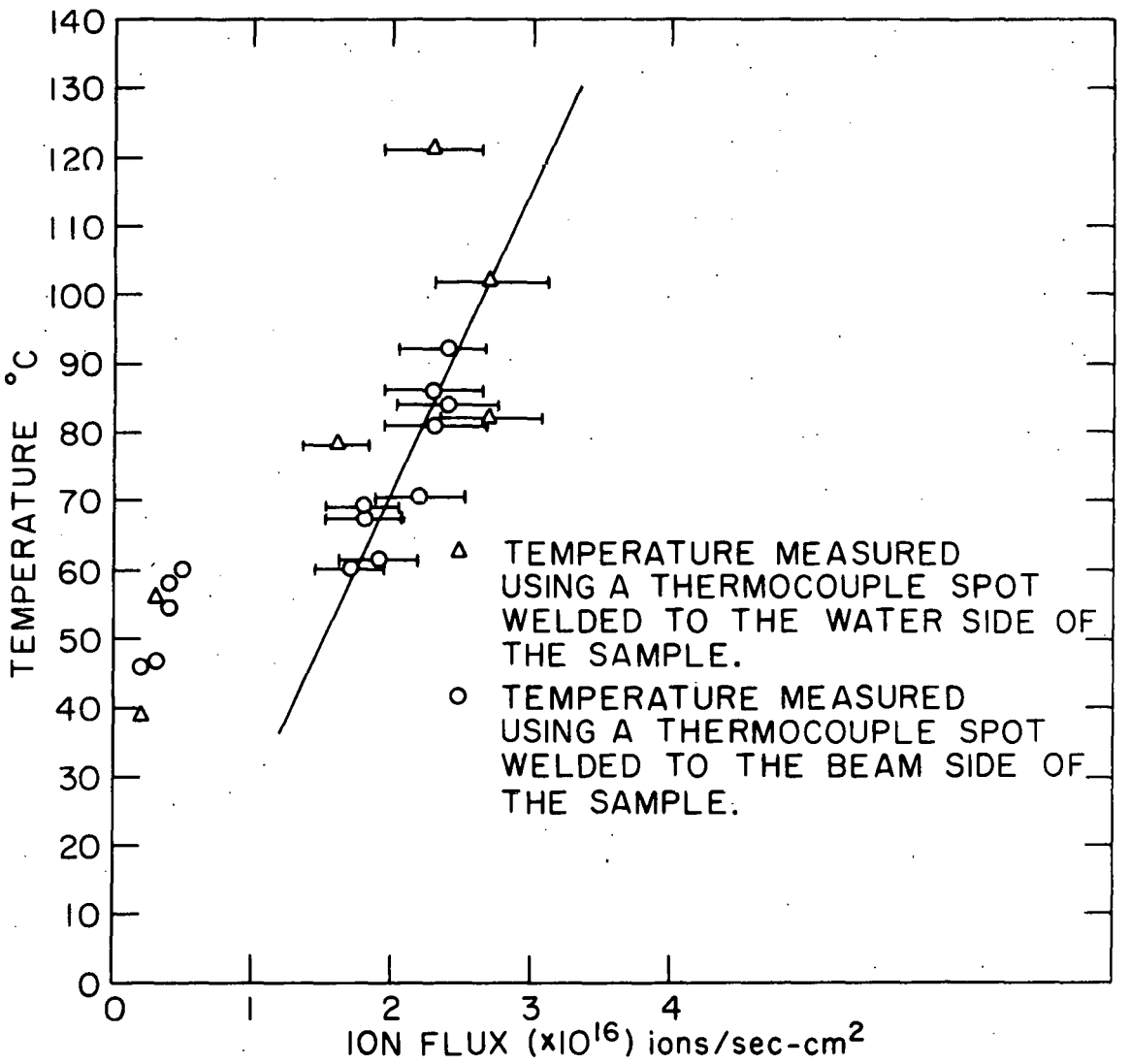

Figure 13. Plot of ion flux versus the temperature of the target sample during irradiation using the data indicated in Table 7

was developed from the measurement systems using spot welded thermocouples as temperature sensors. The error in the temperature values obtained using these systems is not limited to the relatively small error associated with taking a thermocouple reading. Rather, the temperature is subject to fluctuations brought on by changes in the coolant flow rate, proton flux and beam homogeneity.

In order to obtain another point of reference regarding the temperature of the sample, a mock system was developed to try to duplicate the temperature measurement problem under more controlled circumstances. This mock system, represented schematically in Fig. 14, used a spring loaded thermocouple positioned to simulate the temperature measurement system used during sample irradiation.

This mock system provided an indication of the error incurred when a thermocouple bead was subject to coolant flow. The system was set to duplicate the coolant flow rate and the temperature readings obtained from the accelerator's spring loaded thermocouple during irradiation. The end cap and thermocouple used in the mock system were of the same design as the accelerator's end cap and thermocouple. During proton bombardment with an ion flux determined to be approximately $3(10^{16})$ ions/sec-sq cm, the temperature indicated by the spring loaded thermocouple was 41°C to 44°C.

When the mock system's spring loaded thermocouple was brought to a similar temperature reading, the temperature

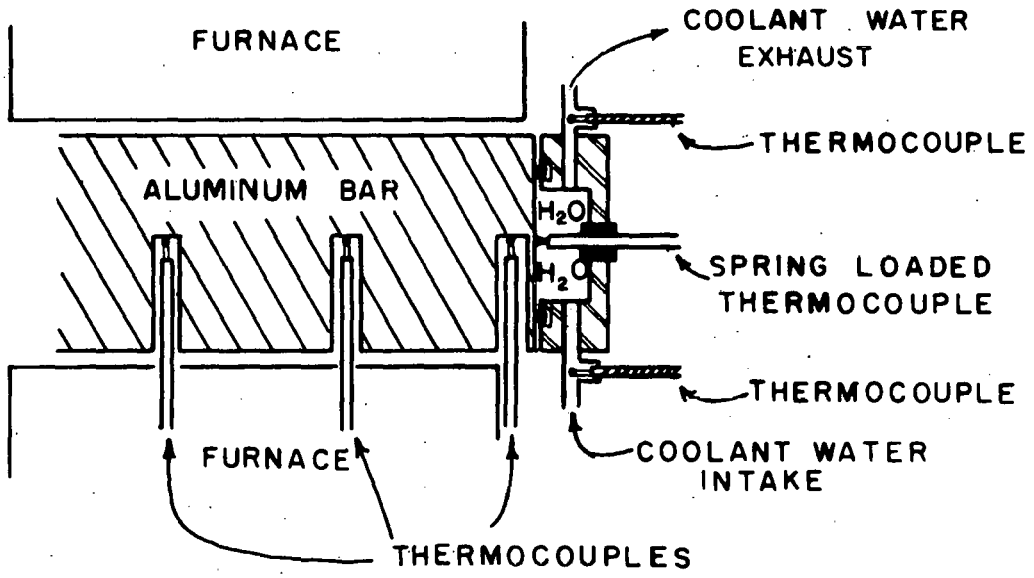

Figure 14. Schematic representation of the mock system used to simulate the temperature measurement problems during irradiation

measured at a position two millimeters into the aluminum bar was 135°C under equilibrium conditions.

The results of experimentation with the mock system indicate acceptable correlation to the temperature values suggested in Fig. 13. The results of these studies reveal that, for an ion flux of $3(10^{16})$ ions/sec-sq cm, the temperature of the sample's beam side can be estimated at 125 $\pm$ 15°C. When the ion flux is decreased to approximately $3(10^{15})$ ions/sec-sq cm, the temperature can be estimated at 45 $\pm$ 15°C.

III. EXPERIMENTAL RESULTS

Some of the factors contributing to the formation of radiation blistering include ion fluence, ion flux, projectile energy, irradiation temperature and orientation of the sample with respect to the beam. Since polycrystalline samples were used, this research was not suited to controlled investigations of the dependence of blister formation on specimen orientation. Irradiation parameters which would reproducibly produce blistered samples were determined. A summary of the irradiation parameters for all samples studied is provided in Table 8. These parameters were used to calculate the projectile flux and fluence for each sample.

$$\text{Ion flux} = \frac{1.6(10^{16})\ \text{ions/coulomb} \times \text{beam current}}{\text{Beam cross sectional area}}$$

$$\text{Ion fluence} = \text{ion flux} \times \text{beam time}$$

The blistered region of a sample was readily apparent as a spot etched onto the sample's polished surface. Visual interpretation of the beam spot appearance for each sample is presented in Table 9. From this information an ion fluence threshold for blister formation was estimated. However, ion flux and projectile energy blistering thresholds could not be defined using the data available. This research employed a projectile energy of 150 Kev, and, for the ion flux values studied, blister formation took place at dose levels of

Table 8. Irradiation parameters and calculated values for ion flux and fluence

Sample number	Beam energy (Kev)	Beam current (ma)	Beam diam. (cm)	Beam time (sec)	Ion flux (ions sec-cm^2)	Ion fluence (ions/cm^2)	Estimated[a] ion fluence
V-1	150	1.0	0.7	1800	$4.2(10^{16})$	$7.5(10^{19})$	$6.4(10^{19})$
V-2	"	"	2.0	180	$5.1(10^{15})$	$9.2(10^{17})$	$7.8(10^{17})$
V-3	"	"	2.0	900	$5.1(10^{15})$	$4.6(10^{18})$	$3.9(10^{18})$
V-4	"	"	2.0	5400	$5.1(10^{15})$	$2.7(10^{19})$	$2.3(10^{19})$
V-5	"	"	1.0	1800	$2.0(10^{16})$	$3.6(10^{19})$	$3.1(10^{19})$
V-6	"	"	0.8	2700	$3.2(10^{16})$	$8.6(10^{19})$	$7.3(10^{19})$
V-7	"	"	0.8	2250	"	$7.2(10^{19})$	$6.1(10^{19})$
V-8	"	"	0.8	1800	"	$5.8(10^{19})$	$4.9(10^{19})$
V-9	"	"	0.8	1350	"	$4.3(10^{19})$	$3.7(10^{19})$
V-10	"	"	0.9	2250	$2.7(10^{16})$	$6.1(10^{19})$	$5.2(10^{19})$
V-11	"	"	0.9	1800	"	$4.9(10^{19})$	$4.2(10^{19})$
V-12	"	0.1	0.8	19560	$3.2(10^{15})$	$6.3(10^{19})$	$5.4(10^{19})$
V-13	"	0.1	0.8	9000	$3.2(10^{15})$	$2.9(10^{19})$	$2.5(10^{19})$
Nb-1	"	1.0	0.6	1800	$5.6(10^{16})$	$1.0(10^{20})$	$8.5(10^{19})$
Mo-1	"	1.0	2.0	1800	$5.1(10^{15})$	$9.2(10^{18})$	$7.8(10^{18})$
Mo-2	"	1.0	1.1	1140	$1.7(10^{16})$	$1.9(10^{19})$	$1.6(10^{19})$

[a]The estimated ion fluence was determined by taking 85% of the ion fluence value indicated in column 7. This estimation reflects the component of the beam which remained invisible during irradiation and was not represented in the beam diameter measurement in column 4.

Table 9. Visual appearance of samples after irradiation

Sample number	Beam diameter (cm)	Beam spot area (cm^2)	Diameter of blistered region (cm)	Visual extent of blistered region[a] (blister spot development)
V-1	0.7	0.4	0.5	Blistered area well defined
V-2	2.0	3.1	---	No evidence of blistering
V-3	2.0	3.1	---	"
V-4	2.0	3.1	---	"
V-5	1.0	0.8	---	Slight evidence of blistering
V-6	0.8	0.5	0.8	Blistered area well defined
V-7	0.8	0.5	0.7	"
V-8	0.8	0.5	0.7	"
V-9	0.8	0.5	0.6	Partially developed spot
V-10	0.9	0.6	0.7	Blistered area well defined
V-11	0.9	0.6	0.6	Partially developed spot
V-12	0.8	0.5	0.5	Blistered area well defined
V-13	0.8	0.5	0.2	"
Nb-1	0.6	0.3	0.3	"
Mo-1	2.0	3.1	---	No evidence of blistering
Mo-2	1.1	1.0	0.4	Blistered area well defined

[a]The visual extent of blistering as apparent to the naked eye.

$2.5(10^{19})$ or greater.

The samples studied fall into three groups. Samples V6, V7, V8, V9, V12 and V13 were prepared as indicated previously, which provides an annealed sample for bombardment. However, samples V10 and V11 were left in a cold worked state. Finally, samples V12 and V13 were bombarded with a beam current of 0.1 ma; whereas, all other samples were bombarded with a beam current of 1.0 ma.

The results of the investigations on a cross section of sample V7 revealed the presence of a small amount of hydride phase. Fig. 15 contains photographs showing the surface relief characteristic of hydride platelet formation. These platelets became apparent upon cooling to -67 $\pm$ 3°C, and would disappear and reappear upon temperature cycling between -67°C and room temperature. The sample's hydride transformation temperature denotes a hydrogen concentration of approximately 50 PPM by weight based on experimentation carried out by Owen and Scott (21). Microscopic examination of the V7 cross section revealed few hydride platelets, and the platelets which were observed tended to be located near the bombarded surface.

A. Blister Appearance

The photographs in Figs. 7 through 12b show portions of the blistered regions for each sample studied. Variations in blister appearance can be attributed to variations in irradiation parameters between specimens, the location of the photo-

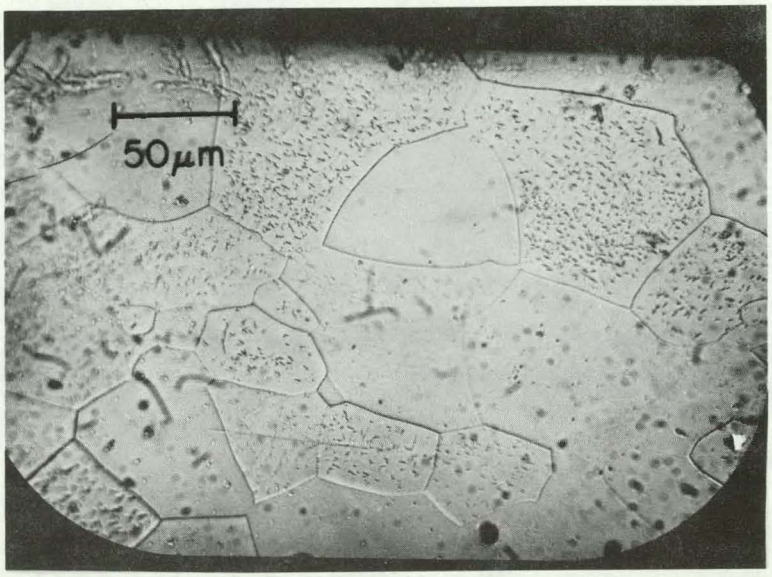

No hydrides visible at room temperature

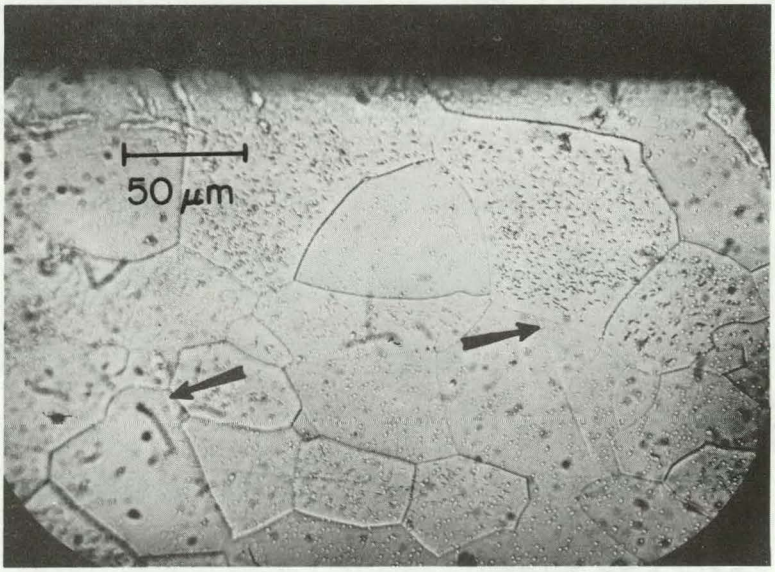

Hydrides visible after cooling below room temperature

Figure 15 **The presence of hydrides is indicated in these photomicrographs of a cross-section of the blistered region for sample V7. The edge visible at the top of the photographs is the "side view" of the bombarded surface**

graphed area within the beam spot and variations in the type of material irradiated. Prior to sample irradiation, S.E.M. examination revealed the polished surface to be smooth up to the resolution limit of 200 Å except for the presence of grain boundaries.

Observations of the blistered regions revealed no suggestion of preferred sites for blister formation. Samples were blistered reasonably uniformly across each grain. Individual blisters did not extend across grain boundaries. Generally, the blister character did not change appreciably between neighboring grains; however, occasionally an isolated grain would show little or no indication of blistering.

The most noticeable trend apparent during observation of a blistered region was the decrease in the severity of the blistering between the center and the edge of the beam spot. This trend is apparent in the photograph sequence for sample V12 shown in Figs. 10a, 10b and 10c. Sample V12 exhibited severe blistering at the center of the beam spot with an obvious decline in blistering severity toward the edge of the beam spot.

Figs. 4 through 6 contain photographs of the blistered region of three samples shown at moderate magnification. These samples represent variations in beam current and material preparation. The appearance of the blisters in each photograph is similar; however, the individual grains are visible in the annealed samples and obvious variations in blistering tendency are apparent between grains. The cold

worked sample shows no indication of grain structure, and blistering is uniform throughout the photograph. The variation in the beam current between the samples in Figs. 4 and 6 did not have a noticeable effect on blister character.

Generally, the blisters appeared as slight surface bulges resembling circular domes with no indication of a direction of preferred development. Many of the blisters were broken, leaving only a crater surrounded by flakes of material which once made up the blister dome. These domes and craters were suited to diameter measurement; however, certain regions of a sample's blister field were so severely blistered that blister diameter measurements were impractical.

Examination of the photographs suggests that as the blisters grew their circular shape was distorted by intersections with other blisters. Eventually, after severe blistering, photographic evidence suggested that large areas would develop as a single blister covering entire grains. These large blisters would usually be mottled with scars from earlier blistering episodes.

IV. DISCUSSION

Measurement of blister size and density provides fairly representative information regarding the severity of blistering; yet, certain aspects of blistering may not be reflected. Blister size and density do not indicate the number of fractured blister domes, the presence of widespread flaking, blister agglomeration or the formation of blisters in craters left by other blisters. In addition, meaningful examination of the critical dose required for blister formation, blister size and blister density is subject to significant variation depending on material and irradiation conditions. In this research, the bombardment of vanadium, niobium and molybdenum with 150 Kev protons produced severely blistered surfaces. Proton fluxes ranged from $3(10^{15})$ to $3(10^{16})$ ions/sec-sq cm with ion fluences ranging from $8(10^{17})$ to $7(10^{19})$ ions/sq cm. This research focused on radiation blistering of vanadium metal at temperatures below the hydride dissociation temperature.

For comparison, previous investigations of annealed polycrystalline vanadium bombarded with 2 Mev He^+ and D^+ at 700°C produced blister diameters of 5 to 8 μm for a dose of $6.2(10^{18})$ He^+/sq cm and 0.5 μm and smaller for a dose of $1.2(10^{19})$ D^+/sq cm (7). 0.5 Mev He^+ irradiations of annealed vanadium at 900°C for doses of $6.2(10^{17})$ and $6.2(10^{18})$ He^+/sq cm produced mean blister diameters of 6.2 μm and 7.4 μm (8). In addition,

variations in projectile flux from approximately 10^{13} to 10^{15} He^+/sq cm produced an increase in blister density from approximately $1(10^4)$ to $7(10^4)$ blisters/sq cm (8).

The studies described above were carried out at temperatures 500°C to 700°C higher than the hydride dissociation temperature for vanadium. As the irradiation temperature is increased, the blister size would be expected to be greater and the critical formation dose would be expected to decrease, which can be associated with the temperature dependence of the material's yield strength. In addition, a higher projectile energy will affect the formation of blisters. Das and Kaminsky's discussion (7,9) of gas pressures inside blisters indicates an increase in blister size with increasing projectile energy. Higher projectile energies correspond to increased blister skin thicknesses. A blister's internal gas pressure is approximately proportional to total particle dose, blister skin thickness and the inverse square of the blister radius. Therefore, if the blister height, particle dose and gas pressure are held constant, the radius would be expected to increase with increasing projectile energy.

This research produced blister diameters on vanadium which ranged between 1 μm and 2 μm after 150 Kev proton irradiation. The blister diameter increased as the total dose was increased (see Fig. 16 and Fig. 17), in agreement with trends indicated by other blistering studies (7-11). In addi-

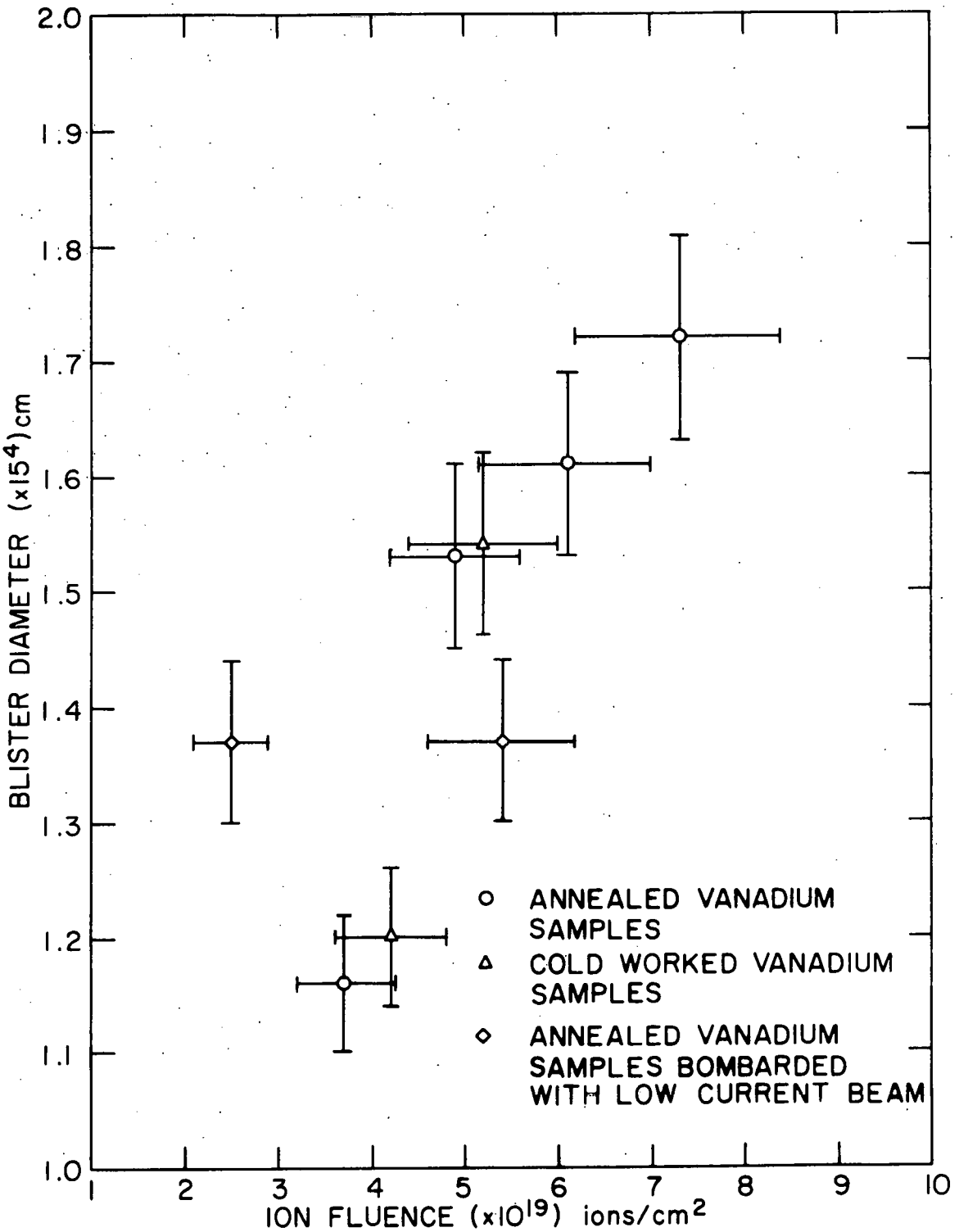

Figure 16. Plot of ion fluence versus mean blister diameter using the values indicated in Table 4

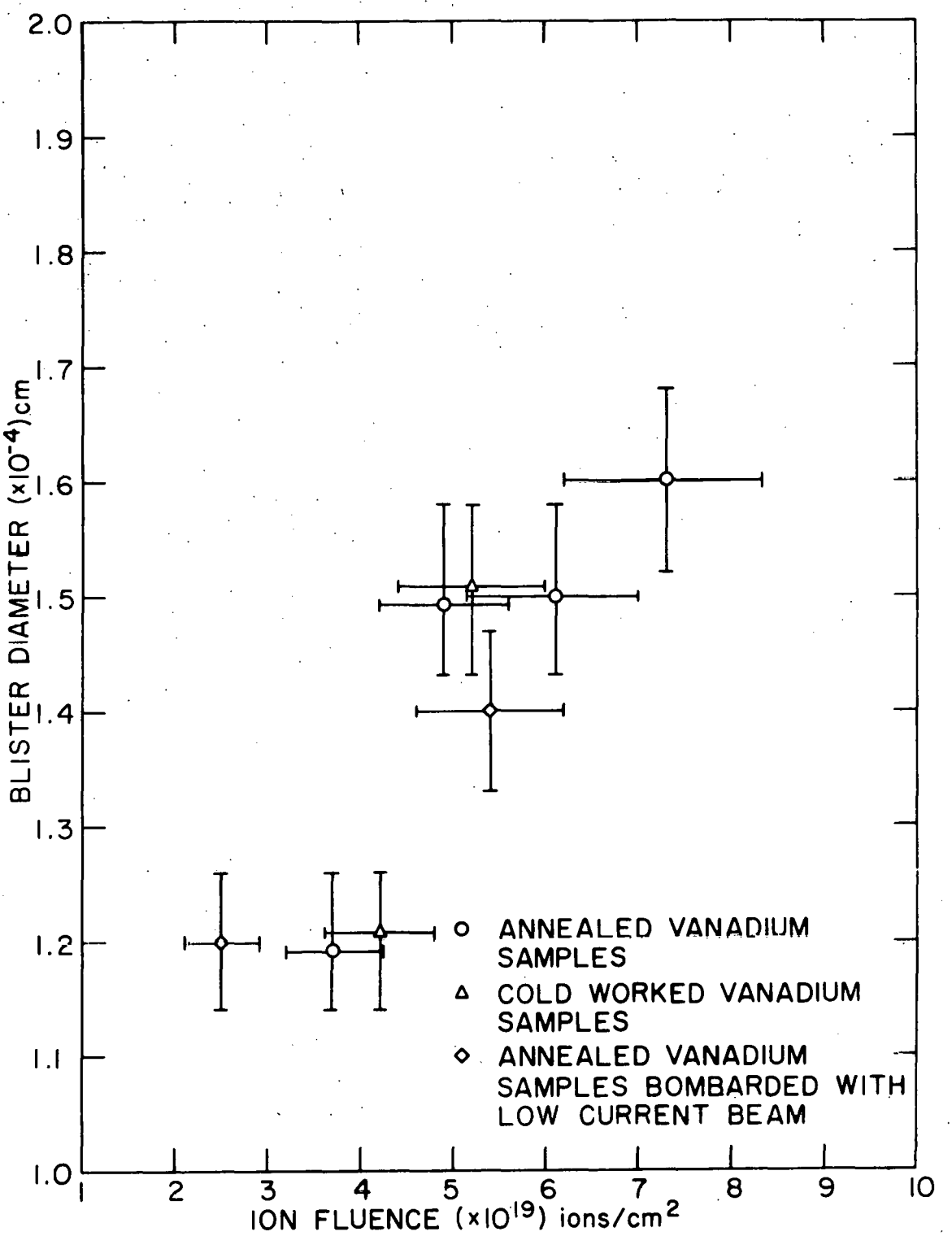

Figure 17. Plot of ion fluence versus the graphically determined blister diameter using the values indicated in Table 4

tion, the mean blister density decreased from $11.5(10^3)$ to $5.5(10^3)$ blisters/sq cm as the total dose was increased (see Fig. 18). This decrease can be associated with the agglomeration of blisters under conditions of severe blistering.

This research produced blistered surfaces on vanadium at ion fluences of $2.5(10^{19})$ H^+/sq cm and greater (see Table 3). Thomas and Bauer (14) irradiated vanadium at 115°C with 150 Kev protons using a flux of $1.25(10^{15})$ H^+/sec-sq cm for doses up to $1.5(10^{19})$ H^+/sq cm without producing blisters. The absence of blister production during their work could be attributed to the lower proton flux and lower total dose compared with the present work. The lower flux would promote a lower damage production rate which could effect hydrogen trapping, while the lower total dose would provide less hydrogen for trapping; therefore, the failure to produce blisters suggests that the gas pressures generated due to supersaturation of the metal during irradiation were insufficient to cause blistering.

During irradiation, the deposition of hydrogen in a narrow region below the specimen surface could result in locally high concentrations of hydrogen. Regions of high hydrogen concentration would normally be dispersed throughout the material by the rapid diffusion of hydrogen, and the dispersal would tend to limit the development of the high internal hydrogen pressures necessary for blister formation.

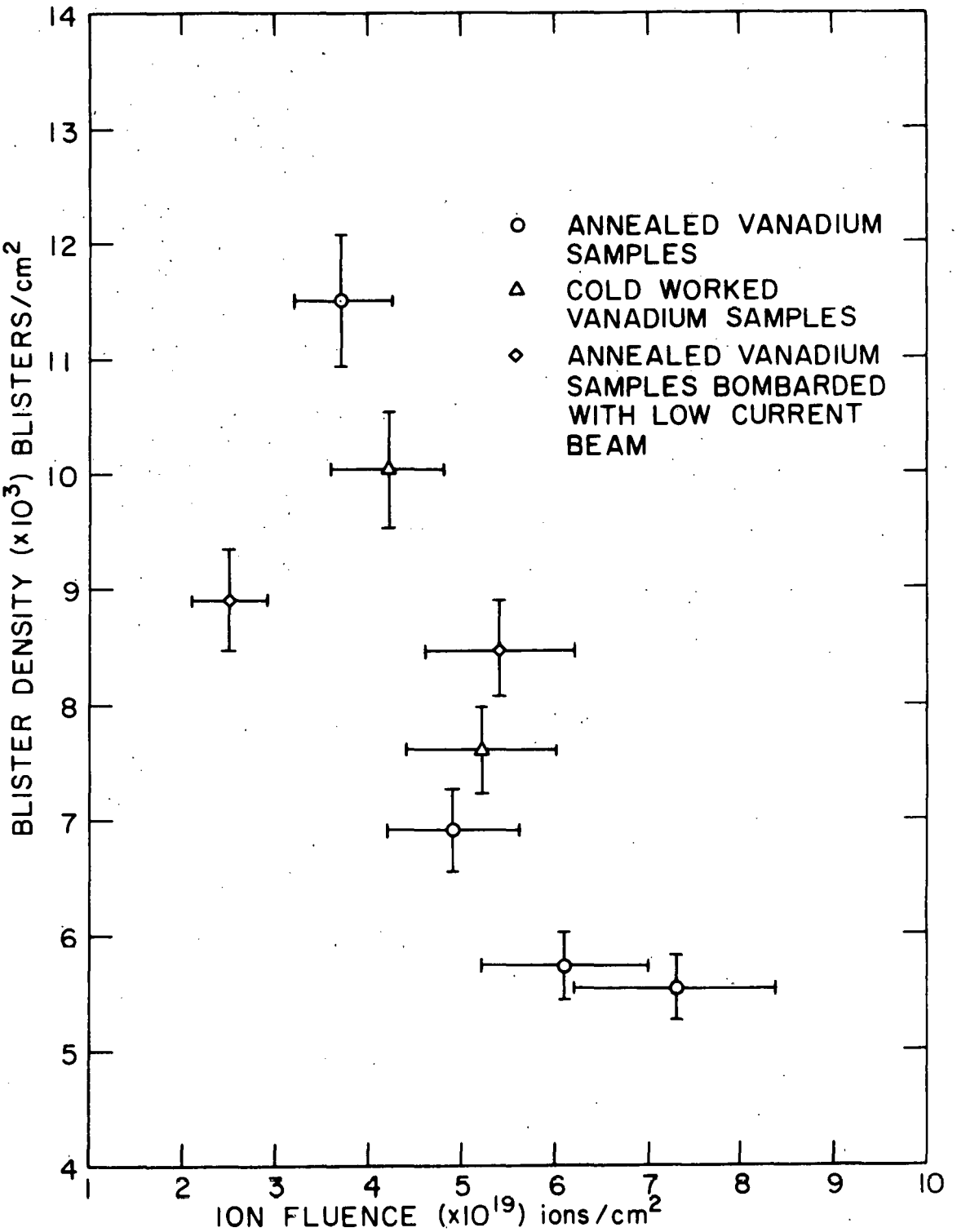

Figure 18. Plot of ion fluence versus mean blister density using the values indicated in Table 6

Studies by Bauer and Thomas (13) have associated the development of blisters and exfoliated surfaces with the release of hydrogen gas. Since the build up of hydrogen gas can be related to blister formation, the dispersal of hydrogen must be limited, implying a decrease in hydrogen diffusion resulting from the method of deposition.

During irradiation tens of defects could be produced per incident particle (6). The deposited hydrogen can become trapped at these defects while diffusing through the material. If the activation energy for release from the trapping sites was greater than the energy required for normal interstitial diffusion, diffusion of hydrogen would be impeded. Experimentation involving 18 Kev D^+ irradiation of nickel by Erents and McCracken (6) revealed a decrease in the diffusion coefficient for deutrium in nickel. This result would tend to support the aforementioned description of diffusion impedance. The development of molecular hydrogen could further impede diffusion and help stabilize regions of high gas pressure.

Under equilibrium conditions, excess hydrogen in vanadium would be expected to form hydride at temperatures below the hydride dissociation temperature of 200°C (3). The production of hydride would inhibit the development of high internal gas pressures associated with blistering. The sample temperature during irradiation was determined to range between 45 $\pm$ 15°C and 125 $\pm$ 15°C depending upon the proton flux (see Fig. 13).

The temperature increased as the proton flux was increased. Since all irradiations were carried out well below the hydride dissociation temperature, the contribution of excess hydrogen to blister formation instead of hydride formation is confounding. Evidently, the irradiation conditions used in this investigation produced severe nonequilibrium conditions.

This behavior can be rationalized if the increased vacancy concentration associated with displacements generated by collisions between energetic protons and lattice atoms could be viewed as an effective temperature. This effective temperature could correspond to the temperature required to reproduce the vacancy concentration in the sample's bombarded region under equilibrium conditions. The characteristic hydrogen solubility and phase transformations could be subject to this effective temperature. Therefore, at effective temperatures above the hydride dissociation temperature, hydrogen gas could be present; whereas, the actual temperature would require the presence of hydride.

Consequentially, the ability of a metal to form a hydride will not prevent blister formation at temperatures below the hydride dissociation temperature under certain nonequilibrium conditions.

V. SUMMARY

In this research, general conditions for blistering were determined, and blistered surfaces were produced on vanadium, niobium and molybdenum. Increases in proton fluence resulted in increases of blister diameter, the number of fractured blister domes and the spallation of the metal surface. In general, the blister characteristics apparent during observation of the blistered regions and the trends ascribed to the formation and growth of the blisters agreed with other blistering studies. However, blisters were formed during proton bombardment at temperatures below the hydride dissociation temperature. The formation of these blisters suggests a variation from the equilibrium phase relationships to allow for the development of internal hydrogen gas pressures suitable for blistering.

VI. BIBLIOGRAPHY

1. F. L. Vook, Physics Today, 28, 34-40 (Sept. 1975).

2. A. P. Fraas and H. Postma, "Preliminary Appraisal of the Hazards Problems of a D-T Fusion Reactor Power Plant," ORNL-TM-2822, Nov. 1970.

3. T. E. Scott, "Hydrogen Embrittlement and Other Effects in Thermonuclear Reactor Materials," IS-3634, Iowa State ERDA, Ames, Iowa, June 1975.

4. D. Steiner, "Tokamak Fusion Reactor," in Fusion Reactor First Wall Materials Meeting AEC-Germantown, USAEC Rept. No. WASH 1206, L. C. Ianniello, Ed., Washington, D.C., U.S. Government Printing Office, April 1972, p. 1.

5. G. M. McCracken, D. K. Jefferies and P. Goldsmith, "The Temperature Dependence of Deutrium Ion Trapping in Niobium, Titanium, Zirconium and Erbium," CLM-P166, UKAEA Culham Lab., Abingdon, Berkshire, Proc. 4th Int. Vacuum Congr., (London: Institute of Physics and Physical Society), 149-154 (March 1968).

6. K. Erents and G. M. McCracken, Brit. J. Appl. Phys. (J. Phys. D.), 2, Ser. 2, 1397-1405 (1969).

7. S. K. Das and M. Kaminsky, J. Nucl. Mater., 53, 115-126 (1974).

8. S. K. Das and M. Kaminsky, International Conference on "Applications of Ion Beams to Metals," CONF-731028-3, Alburquerque, New Mexico, October 2-4, 1973.

9. S. K. Das and M. Kaminsky, J. Appl. Phys., 44, No. 1, 23-31 (Jan. 1973).

10. S. K. Das and M. Kaminsky, J. Appl. Phys., 44, No. 6, 2520-2529 (June 1973).

11. M. Kaminsky and S. K. Das, Appl. Phys. Lett., 21, No. 9, 443-445 (Nov. 1972).

12. G. L. Kulcinski and G. A. Emmert, J. Nucl. Mater., 53, 31-38 (1974).

13. W. Bauer and G. J. Thomas, J. Nucl. Mater., 53, 127-133 (1974).

14. G. J. Thomas and W. Bauer, J. Nucl. Mater., 53, 134-141 (1974).

15. G. A. Nelson and R. T. Effinger, Welding J. Res. Suppl., 34, 12-15 (1955).

16. A. S. Tetelman and W. D. Robertson, Trans. AIME, 224, 775-783 (1962).

17. A. S. Tetelman and W. D. Robertson, Acta Met., 11, 415-426 (1963).

18. F. DeKazinczy, Jernkontorets Annaler, 140, 347-359 (1956).

19. O. N. Carlson and C. V. Owen, J. Electrochemical Soc., 108, No. 1, 88-93 (Jan. 1961).

20. D. H. Sherman, C. V. Owen and T. E. Scott, Trans. Met. Soc. of AIME, 242, 1775-1784 (Sept. 1968).

21. C. V. Owen and T. E. Scott, Met. Trans., 3, 1715-1726 (July 1972).

VII. ACKNOWLEDGMENTS

The author is grateful to all those who contributed their efforts to this investigation. Sincere appreciation is extended to Dr. Tom Scott for serving as major professor, for his guidance and for his encouragement throughout this investigation and the author's entire graduate program. Special thanks are extended to Wayne Stensland and Lowell Mathison for the maintenance and operation of the accelerator facility, to Ed Gibson for operating the S.E.M. and to Lester Reed, Harlan Baker and Chuck Owen for their good humor and assistance with sample preparation and a variety of laboratory procedures. Finally, thanks to Verna Thompson for her excellent typing and valuable assistance in the assembly of this thesis.

VIII. APPENDIX A

This appendix contains the raw blister measurement data used in the development of Tables 2, 3 and 5. These measurements were made using a Carl-Zeiss Particle Analyzer, and are presented in Tables A1 through A25 along with the pertinent information regarding photomicrograph magnification.

Information in Table 2 was developed by taking the arithmetic mean of the diameter values for each photomicrograph based on the mean value for each measurement range. Figures A1 through A8 contain representative samples of the blister size distribution curves used to generate the blister diameter values presented in Table 3. The total number of blisters indicated for each photomicrograph was used along with the photograph area (i.e. 76 sq cm) and the photomicrograph magnification to develop the blister density values presented in Table 5.

Table A1. Raw blister diameter measurements from photomicrograph numbers 1 and 2 for sample V-6

Measured blister diameter range[a] (mm)	Number of blisters in each diameter range		Measured blister diameter range[a] (mm)	Number of blisters in each diameter range	
	Photo 1	Photo 2		Photo 1	Photo 2
2.32-2.87	1	0	9.46-10.04	3	1
2.87-3.42	1	4	10.04-10.60	2	5
3.42-3.97	1	4	10.60-11.15	6	1
3.97-4.52	9	5	11.15-11.70	2	2
4.52-5.08	4	18	12.25-12.80	0	1
5.08-5.63	6	14	12.80-13.36	0	1
5.63-6.18	13	11	13.36-13.91	2	0
6.18-6.73	11	8	13.91-14.46	0	1
6.73-7.28	6	13	14.46-15.01	1	0
7.28-7.84	8	10	15.56-16.12	0	1
7.84-8.39	6	1	16.12-16.67	1	0
8.39-8.94	4	5			
8.94-9.46	10	3			
Total number of blisters per photo				97	109

[a]Magnification factor: Photomicrograph number 1 = 3850X
Photomicrograph number 2 = 3850X.

Table A2. Raw blister diameter measurements from photomicrograph numbers 4 and 5 for sample V-6

Measured blister diameter range[a] (mm)	Number of blisters in each diameter range		Measured blister diameter range[a] (mm)	Number of blisters in each diameter range	
	Photo 4	Photo 5		Photo 4	Photo 5
1.76-2.32	1	0	7.84-8.39	8	1
2.32-2.87	0	4	8.39-8.94	5	0
2.87-3.42	4	8	8.94-9.46	6	0
3.42-3.97	5	22	9.46-10.04	2	0
3.97-4.52	15	27	10.04-10.60	5	0
4.52-5.08	9	24	10.60-11.15	1	1
5.08-5.63	17	24	11.70-12.25	1	0
5.63-6.18	10	22	12.80-13.36	1	0
6.18-6.73	13	12	14.46-15.01	1	0
6.73-7.28	18	2	15.01-15.56	1	0
7.28-7.84	4	1	----------	-	-
Total number of blisters per photo				127	148

[a]Magnification factors: Photomicrograph number 4 = 3850X
Photomicrograph number 5 = 3850X.

Table A3. Raw blister diameter measurements from photomicrograph numbers 6 and 7 for sample V-6

Measured blister diameter range[a] (mm)	Number of blisters in each diameter range		Measured blister diameter range[a] (mm)	Number of blisters in each diameter range	
	Photo 6	Photo 7		Photo 6	Photo 7
2.32-2.87	0	1	11.70-12.25	2	1
2.87-3.42	2	2	12.25-12.80	1	0
3.42-3.97	2	8	12.80-13.36	2	1
3.97-4.52	1	8	13.36-13.91	2	0
4.52-5.08	3	5	13.91-14.46	1	1
5.08-5.63	8	7	15.01-15.56	1	0
5.63-6.18	6	16	15.56-16.12	1	0
6.18-6.73	9	12	17.77-18.32	0	1
6.73-7.28	8	13	19.43-19.98	0	1
7.28-7.84	10	4	20.53-21.08	0	1
7.84-8.39	5	9	21.08-21.64	0	1
8.39-8.94	5	5	22.19-22.74	0	2
8.94-9.46	3	3	23.29-23.84	0	1
9.46-10.04	3	5	23.84-24.40	0	1
10.04-10.60	4	3	27.16-27.71	0	1
10.69-11.15	6	2			
11.15-11.70	4	0			
Total number of blisters per photo				91	106

[a]Magnification factors: Photomicrograph number 6=3850X
Photomicrograph number 7=3850X.

Table A4. Raw blister diameter measurements from photomicrograph number 2 for sample V-7

Measured blister diameter range[a] (mm)	Number of blisters in each diameter range Photo 2	Measured blister diameter range[a] (mm)	Number of blisters in each diameter range Photo 2
2.87-3.42	1	9.46-10.04	7
3.42-3.97	1	10.04-10.60	5
4.52-5.08	1	10.60-11.15	2
5.08-5.63	1	11.15-11.70	3
5.63-6.18	6	11.70-12.25	1
6.18-6.73	11	12.25-12.80	3
6.73-7.28	7	12.80-13.36	1
7.27-7.84	9	13.91-14.46	2
7.84-8.39	6	15.01-15.56	1
8.39-8.94	4	16.67-17.22	1
8.94-9.46	4	----------	-
Total number of blisters per photo			76

[a]Magnification factor: Photomicrograph number 2 = 5200X.

Table A5. Raw blister diameter measurements from photomicrograph number 3 for sample V-7

Measured blister diameter range[a] (mm)	Number of blisters in each diameter range Photo 3	Measured blister diameter range[a] (mm)	Number of blisters in each diameter range Photo 3
2.87-3.42	3	7.28-7.84	9
3.42-3.97	2	7.84-8.39	7
3.97-4.52	4	8.39-8.94	11
4.52-5.08	6	8.94-9.46	4
5.08-5.63	7	9.46-10.04	4
5.63-6.18	16	10.04-10.60	2
6.18-6.73	11	10.60-11.15	1
6.73-7.28	13	11.15-11.70	1
Total number of blisters per photo			102

[a]Magnification factor: Photomicrograph number 3 = 3800X.

Table A6. Raw blister diameter measurements from photomicrograph number 4 for sample V-7

Measured blister diameter range[a] (mm)	Number of blisters in each diameter range Photo 4	Measured blister diameter range[a] (mm)	Number of blisters in each diameter range Photo 4
1.32-1.51	2	5.19-5.37	10
1.69-1.88	1	5.37-5.56	7
1.88-2.06	1	5.56-.574	7
2.06-2.24	5	5.74-5.92	4
2.24-2.43	4	5.92-6.11	5
2.80-2.98	1	6.11-6.29	8
3.16-3.35	3	6.29-6.48	4
3.53-3.72	1	6.48-6.66	3
3.72-3.90	5	6.66-6.84	3
3.90-4.08	4	6.84-7.03	2
4.08-4.27	6	7.03-7-21	2
4.27-4.45	4	7.21-7.40	2
4.45-4.64	5	7.40-7.58	1
4.64-4.82	6	8.13-8.32	1
4·82-5.00	6	9.05-9.24	1
5.00-5.19	9	---	--
Total number of blisters per photo			123

[a]Magnification factor: Photomicrograph number 4 = 3800X.

Table A7. Raw blister diameter measurements from photomicrograph numbers 5 and 6 for sample V-7

Measured blister diameter range[a] (mm)	Number of blisters in each diameter range		Measured blister diameter range[a] (mm)	Number of blisters in each diameter range	
	Photo 5	Photo 6		Photo 5	Photo 6
2.61-2.80	2	0	5.92-6.11	13	4
3.16-3.35	1	0	6.11-6.29	9	4
3.35-3.53	2	0	6.29-6.48	6	7
3.53-3.72	3	0	6.48-6.66	1	5
3.72-3.90	0	2	6.66-6.84	7	8
3.90-4.08	4	1	6.84-7.03	4	1
4.08-4.27	3	2	7.03-7.21	3	8
4.27-4.45	5	0	7.21-7.40	4	6
4.45-4.64	9	1	7.40-7.58	4	3
4.64-4.82	4	3	7.58-7.76	3	2
4.82-5.00	7	4	7.76-7.95	2	2
5.00-5.19	14	2	8.13-8.32	1	2
5.19-5.37	9	2	8.32-8.50	3	0
5.37-5.56	7	3	8.68-8.87	1	2
5.56-5.74	4	5	9.05-9.24	0	5
5.74-5.92	9	7			
Total number of blisters per photo				144	91

[a]Magnification factors: Photomicrograph number 5=3800X
Photomicrograph number 6=3800X.

Table A8. Raw blister diameter measurements from photomicrograph numbers 7 and 8 for sample V-7

Measured blister diameter range[a] (mm)	Number of blisters in each diameter range		Measured blister diameter range[a] (mm)	Number of blisters in each diameter range	
	Photo 7	Photo 8		Photo 7	Photo 8
1.32-1.51	2	0	5.19-5.37	8	2
1.51-1.69	1	0	5.37-5.56	1	8
1.69-1.88	1	0	5.56-5.74	4	6
2.06-2.24	2	0	5.74-5.92	9	5
2.24-2.43	2	0	5.92-6.11	4	7
2.43-2.61	2	0	6.11-6.29	4	4
2.61-2.80	1	0	6.29-6.48	2	4
2.80-2.98	4	0	6.48-6.66	2	5
2.98-3.16	3	3	6.66-6.84	3	4
3.16-3.35	6	0	6.84-7.03	2	3
3.35-3.53	2	1	7.03-7.21	2	3
3.53-3.72	3	0	7.21-7.40	2	1
3.72-3.90	2	2	7.58-7.76	0	1
3.90-4.08	5	2	7.76-7.95	0	1
4.08-4.27	2	4	7.95-8.13	2	0
4.27-4.45	11	3	8.50-8.68	0	1
4.45-4.64	8	2	8.87-9.05	1	1
4.64-4.82	5	1	9.05-9.24	0	3
4.82-5.00	4	3			
5.00-5.19	5	3			
Total number of blisters per photo				177	83

[a]Magnification factors: Photomicrograph number 7=3800X
Photomicrograph number 8=3800X.

Table A9. Raw blister diameter measurements from photomicrograph numbers 1 and 2 for sample V-8

Measured blister diameter range[a] (mm)	Number of blisters in each diameter range		Measured blister diameter range[a] (mm)	Number of blisters in each diameter range	
	Photo 1	Photo 2		Photo 1	Photo 2
2.87-3.42	2	1	7.84-8.39	4	8
3.42-3.97	5	2	8.39-8.94	2	6
3.97-4.52	8	5	8.94-9.46	5	3
4.52-5.08	8	14	9.46-10.04	1	4
5.08-5.63	13	14	10.04-10.60	1	2
5.63-6.18	24	12	10.60-11.15	2	2
6.18-6.73	13	20	11.15-11.70	0	2
6.73-7.28	15	14	11.70-12.25	2	0
7.28-7.84	15	5	12.25-12.80	1	0
			12.80-13.36	0	1
Total number of blisters per photo				121	115

[a]Magnification factors: Photomicrograph number 1-3700X
Photomicrograph number 2=3700X.

Table A10: Raw blister diameter measurements from photomicrograph numbers 3 and 4 for sample V-8

Measured blister diameter range[a] (mm)	Number of blisters in each diameter range		Measured blister diameter range[a] (mm)	Number of blisters in each diameter range	
	Photo 3	Photo 4		Photo 3	Photo 4
2.06-2.24	3	0	5.37-5.56	9	9
2.24-2.43	0	5	5.56-5.74	10	6
2.43-2.61	2	2	5.74-5.92	5	7
2.61-2.80	4	3	5.92-6.11	4	8
2.80-2.98	3	2	6.11-6.29	4	4
2.98-3.16	3	4	6.29-6.48	4	3
3.16-3.35	0	6	6.48-6.66	4	3
3.35-3.53	8	5	6.66-6.84	1	5
3.53-3.72	8	3	6.84-7.03	2	4
3.72-3.90	10	5	7.03-7.21	3	5
3.90-4.08	7	4	7.21-7.40	1	3
4.08-4.27	6	9	7.40-7.58	2	2
4.27-4.45	6	3	7.58-7.76	0	1
4.45-4.64	9	10	7.76-7.95	1	1
4.64-4.82	9	11	7.95-8.13	2	2
4.82-5.00	11	8	8.13-8.32	0	2
5.00-5.19	5	7			
5.19-5.37	10	4			
Total number of blisters per photo				157	159

[a]Magnification factors: Photomicrograph number 3=3700X
Photomicrograph number 4=3700X.

Table A11. Raw blister diameter measurements from photomicrograph numbers 5 and 6 for sample V-8

Measured blister diameter range[a] (mm)	Number of blisters in each diameter range		Measured blister diameter range[a] (mm)	Number of blisters in each diameter range	
	Photo 5	Photo 6		Photo 5	Photo 6
2.06-2.24	1	0	5.56-5.74	10	10
2.61-2.80	2	1	5.74-5.92	11	4
2.80-2.98	2	0	5.92-6.11	6	6
2.98-3.16	2	2	6.11-6.29	4	6
3.16-3.35	3	1	6.29-6.48	6	5
3.35-3.53	3	3	6.48-6.66	1	4
3.53-3.72	5	6	6.66-6.84	2	1
3.72-3.90	2	3	6.84-7.03	1	1
3.90-4.08	6	1	7.03-7.21	0	3
4.08-4.27	9	5	7.21-7.40	0	1
4.27-4.45	12	9	7.40-7.58	1	1
4.45-4.64	11	4	7.58-7.76	0	2
4.64-4.82	9	7	7.76-7.95	0	3
4.82-5.00	17	3	8.32-8.50	1	1
5.00-5.19	14	11	8.50-8.68	0	1
5.19-5.37	14	9	8.68-8.87	0	2
5.37-5.56	8	3	8.87-9.05	0	1
			9.05-9.24	0	4
Total number of blisters per photo				164	124

[a]Magnification factors: Photomicrograph number 5=3700X
Photomicrograph number 6=3700X.

Table A12. Raw blister diameter measurements from photomicrograph number 7 for sample V-8

Measured blister diameter range[a] (mm)	Number of blisters in each diameter range Photo 7	Measured blister diameter range[a]	Number of blisters in each diameter range Photo 7
3.42-3.97	2	8.39-8.94	6
3.97-4.52	5	8.94-9.49	3
4.52-5.08	14	9.49-10.04	2
5.08-5.63	22	10.04-10.60	3
5.63-6.18	12	10.60-11.15	2
6.18-6.73	18	11.15-11.70	1
6.73-7.28	19	11.70-12.25	1
7.28-7.84	15	12.25-12.80	2
7.84-8.39	12	14.46-15.01	1
Total number of blisters per photo			140

[a]Magnification factor: Photomicrograph number 7 = 3700X.

Table A13. Raw blister diameter measurements from photomicrograph numbers 1 and 3 for sample V-9

Measured blister diameter range[a] (mm)	Number of blisters in each diameter range Photo 1	Photo 3	Measured blister diameter range[a] (mm)	Number of blisters in each diameter range Photo 1	Photo 3
1.14-1.32	0	2	4.64-4.82	15	16
1.88-2.06	1	2	4.82-5.00	11	13
2.06-2.24	3	3	5.00-5.10	9	15
2.24-2.43	3	2	5.19-5.37	3	12
2.43-2.61	8	1	5.37-5.56	6	9
2.61-2.80	18	3	5.56-5.74	2	6
2.80-2.98	19	12	5.74-5.92	1	11
2.98-3.16	17	3	5.92-6.11	2	10
3.16-3.35	31	8	6.11-6.29	3	8
3.35-3.53	23	13	6.29-6.48	0	5
3.53-3.72	31	9	6.48-6.66	0	2
3.72-3.90	21	8	6.66-6.84	0	3
3.90-4.08	33	10	6.84-7.03	0	3
4.08-4.27	14	18	7.03-7.21	0	1
4.27-4.45	22	18	8.68-8.87	0	1
4.45-4.64	21	15			
Total number of blisters per photo				317	242

[a]Magnification factors: Photomicrograph number 1=3600X
Photomicrograph number 2=3600X

Table A14. Raw blister diameter measurements from photomicrograph number 2 for sample V-9

Measured blister diameter range[a] (mm)	Number of blisters in each diameter range Photo 2	Measured blister diameter range[a] (mm)	Number of blisters in each diameter range Photo 2
3.97-4.52	4	8.94-9.49	4
4.52-5.08	6	9.49-10.04	1
5.08-5.63	4	10.04-10.60	3
5.63-6.18	11	10.60-11.15	8
6.18-6.73	6	11.15-11.70	3
6.73-7.28	8	11.70-12.25	3
7.28-7.84	13	12.80-13.36	1
7.84-8.39	8	16.12-16.67	1
8.39-8.94	7	----------	-
Total number of blisters per photo			91

[a]Magnification factor: Photomicrograph number 2 = 7000X.

Table A15. Raw blister diameter measurements from photomicrograph numbers 2 and 4 for sample V-10

Measured blister diameter range[a] (mm)	Number of blisters in each diameter range		Measured blister diameter range[a] (mm)	Number of blisters in each diameter range	
	Photo 2	Photo 4		Photo 2	Photo 4
2.06-2.24	1	0	5.74-5.92	3	5
2.24-2.43	1	0	5.92-6.11	4	6
2.43-2.61	1	0	6.11-6.29	3	8
2.80-2.98	0	2	6.29-6.48	5	3
2.98-3.16	0	4	6.48-6.66	8	6
3.16-3.35	0	2	6.66-6.84	2	3
3.35-3.53	5	1	6.84-7.03	4	3
3.53-3.72	1	7	7.03-7.21	3	2
3.72-3.90	1	1	7.21-7.40	3	3
3.90-4.08	8	6	7.40-7.58	1	1
4.08-4.27	5	5	7.58-7.76	1	3
4.27-4.45	7	5	7.76-7.95	3	6
4.45-4.64	1	4	7.95-8.13	1	0
4.64-4.82	6	7	8.13-8.32	3	2
4.82-5.00	9	7	8.32-8.50	1	1
5.00-5.19	4	3	8.50-8.68	1	0
5.19-5.37	5	7	8.68-8.87	1	0
5.37-5.56	7	9	8.87-9.05	1	0
5.56-5.74	3	8	9.05-9.24	8	5
Total number of blisters per photo				176	280

[a]Magnification factors: Photomicrograph number 5=3800X
Photomicrograph number 6=3800X.

Table A16. Raw blister diameter measurements from photomicrograph number 3 for sample V-10

Measured blister diameter range[a] (mm)	Number of blisters in each diameter range Photo 3	Measured blister diameter range[a] (mm)	Number of blisters in each diameter range Photo 3
1.76-2.32	1	7.28-7.84	6
2.32-2.87	2	7.84-8.39	1
2.87-3.42	9	8.39-8.94	3
3.42-3.97	7	8.94-9.49	5
3.97-4.52	16	9.49-10.04	1
4.52-5.08	24	10.04-10.60	1
5.08-5.63	22	10.60-11.15	1
5.63-6.18	29	11.70-12.25	1
6.18-6.73	12	12.25-12.80	1
6.73-7.28	7		
Total number of blisters per photo			150

[a]Magnification factor: Photomicrograph number 3=3800X.

Table A17. Raw blister diameter measurements from photomicrograph numbers 5 and 6 for sample V-10

Measured blister diameter range[a] (mm)	Number of blisters in each diameter range		Measured blister diameter range[a] (mm)	Number of blisters in each diameter range	
	Photo 5	Photo 6		Photo 5	Photo 6
1.51-1.69	0	1	5.56-5.74	10	6
2.06-2.24	0	4	5.74-5.92	3	5
2.24-2.43	3	6	5.92-6.11	8	1
2.43-2.61	0	2	6.11-6.29	11	1
2.61-2.80	2	4	6.29-6.48	6	3
2.80-2.98	3	8	6.48-6.66	13	1
2.98-3.16	1	14	6.66-6.84	2	2
3.16-3.35	4	13	6.84-7.03	2	0
3.35-3.53	4	11	7.03-7.21	1	0
3.53-3.72	3	29	7.21-7.40	2	1
3.72-3.90	3	22	7.40-7.58	1	0
3.90-4.08	7	13	7.76-7.95	0	1
4.08-4.27	6	20	7.95-8.13	1	0
4.27-4.45	8	29	8.13-8.32	1	0
4.45-4.64	9	17	8.50-8.68	1	0
4.64-4.82	6	17	8.87-9.05	2	0
4.82-5.00	10	16	9.05-9.24	1	0
5.00-5.19	15	17			
5.19-5.37	18	10			
5.37-5.56	9	6			
Total number of blisters per photo				176	280

[a]Magnification factors: Photomicrograph number 5=3800X
Photomicrograph number 6=3800X.

Table A18. Raw blister diameter measurements from photomicrograph numbers 7 and 8 for sample V-10

Measured blister diameter range[a] (mm)	Number of blisters in each diameter range		Measured blister diameter range[a] (mm)	Number of blisters in each diameter range	
	Photo 7	Photo 8		Photo 7	Photo 8
2.87-3.42	1	0	10.60-11.15	4	2
3.42-3.97	2	3	11.15-11.70	3	2
3.97-4.52	5	5	12.25-12.80	3	0
4.52-5.08	7	7	12.80-13.36	1	2
5.08-5.63	12	8	13.36-13.91	1	0
5.63-6.18	6	6	13.91-14.46	1	0
6.18-6.73	7	14	14.46-15.01	2	1
6.73-7.28	5	13	15.01-15.56	1	1
7.28-7.84	4	11	16.12-16.67	1	0
7.84-8.39	3	8	16.67-17.22	1	0
8.39-8.94	3	4	17.22-17.77	1	0
8.94-9.49	5	4	17.77-18.32	1	0
9.49-10.04	1	0	18.88-19.43	1	1
10.04-10.60	4	1	22.74-23.29	1	0
Total number of blisters per photo				84	93

[a]Magnification factors: Photomicrograph number 7=3800X
Photomicrograph number 8=2800X.

Table A19. Raw blister diameter measurements from photomicrograph numbers 1 and 2 for sample V-11

Measured blister diameter range[a] (mm)	Number of blisters in each diameter range Photo 1	Photo 2	Measured blister diameter range[a] (mm)	Number of blisters in each diameter range Photo 1	Photo 2
0.90-1.14	1	0	4.27-4.45	13	10
1.32-1.51	0	1	4.45-4.64	10	13
1.51-1.69	3	1	4.64-4.82	10	10
1.69-1.88	0	2	4.82-5.00	6	10
1.88-2.06	8	7	5.00-5.19	10	13
2.06-2.24	4	4	5.15-5.37	6	6
2.24-2.43	3	3	5.37-5.56	6	4
2.43-2.61	5	14	5.56-5.74	4	2
2.61-2.80	7	6	5.74-5.92	6	4
2.80-2.98	9	19	6.11-6.29	1	3
2.98-3.16	6	16	6.29-6.48	1	5
3.16-3.35	6	12	6.48-6.66	3	3
3.35-3.53	13	16	6.66-6.84	1	1
3.53-3.72	9	16	6.84-7.03	0	2
3.72-3.90	18	9	7.03-7.21	0	1
3.90-4.08	11	12	9.05-9.24	0	1
4.08-9.27	9	12			
Total number of blisters per photo				190	238

[a]Magnification factors: Photomicrograph number 1=3600X
Photomicrograph number 2-3600X.

Table A20. Raw blister diameter measurements from photomicrograph number 3 for sample V-11

Measured blister diameter range[a] (mm)	Number of blisters in each diameter range Photo 3	Measured blister diameter range[a] (mm)	Number of blisters in each diameter range Photo 3
2.24-2.43	1	4.82-5.00	11
2.43-2.61	1	5.00-5.19	10
2.61-2.80	3	5.15-5.37	9
2.80-2.98	3	5.37-5.56	16
2.98-3.16	13	5.56-5.74	13
3.16-3.35	7	5.74-5.92	19
3.35-3.53	6	5.92-6.11	10
3.53-3.72	5	6.11-6.29	5
3.72-3.90	14	6.29-6.48	5
3.90-4.08	7	6.48-6.66	4
4.08-4.27	9	6.66-6.84	3
4.27-4.45	10	6.84-7.03	3
4.45-4.64	18	7.40-7.58	1
4.64-4.82	8		
Total number of blisters per photo			214

[a]Magnification factor: Photomicrograph number 3 = 3600X.

Table A21. Raw blister diameter measurements from photomicrograph numbers 2 and 5 for sample V-12

Measured blister diameter range[a] (mm)	Number of blisters in each diameter range		Measured blister diameter range[a] (mm)	Number of blisters in each diameter range	
	Photo 2	Photo 5		Photo 2	Photo 5
1.21-1.76	0	2	8.94-9.49	3	4
1.76-2.32	0	7	9.49-10.04	2	4
2.32-2.87	0	28	10.04-10.60	7	1
2.87-3.42	0	37	10.60-11.15	5	1
3.42-3.97	0	39	11.15-11.70	4	1
3.97-4.52	0	21	11.70-12.25	4	0
4.52-5.08	0	23	12.25-12.80	3	0
5.08-5.63	1	28	12.80-13.36	0	1
5.63-6.18	2	24	13.36-13.91	1	1
6.18-6.73	0	18	14.46-15.01	1	0
6.73-7.28	5	11	15.01-15.56	1	0
7.28-7.84	4	9	16.12-16.67	1	1
7.84-8.39	6	4	16.67-17.22	1	0
8.39-8.94	7	4	17.77-18.32	1	0
Total number of blisters per photo				62	269

[a]Magnification factors: Photomicrograph number 2=3750X
Photomicrograph number 5=3750X

Table A22. Raw blister diameter measurements from photomicrograph numbers 6 and 7 for sample V-12

Measured blister diameter range[a] (mm)	Number of blisters in each diameter range		Measured blister diameter range[a] (mm)	Number of blisters in each diameter range	
	Photo 6	Photo 7		Photo 6	Photo 7
2.32-2.87	6	7	7.84-8.39	6	1
2.87-3.42	9	19	8.39-8.94	4	2
3.42-3.97	11	23	8.94-9.49	3	0
3.97-4.52	19	28	9.49-10.04	2	0
4.52-5.08	20	20	10.04-10.60	6	0
5.08-5.63	24	15	10.60-11.15	1	0
5.63-6.18	9	7	11.15-11.70	1	0
6.18-6.73	23	5	11.70-12.25	1	0
6.73-7.28	8	3	12.80-13.36	1	1
7.28-7.84	9	7	13.36-13.91	1	0
Total number of blisters per photo				138	164

[a]Magnification factors: Photomicrograph number 6=3750X
Photomicrograph number 7=3750X.

Table A23. Raw blister diameter measurements from photomicrograph numbers 1 and 3 for sample V-13

Measured blister diameter range[a] (mm)	Number of blisters in each diameter range		Measured blister diameter range[a] (mm)	Number of blisters in each diameter range	
	Photo 1	Photo 3		Photo 1	Photo 3
2.32-2.87	2	0	8.39-8.94	5	10
2.87-3.42	5	5	8.94-9.49	2	3
3.42-3.97	14	10	9.49-10.04	1	3
3.97-4.52	14	18	10.04-10.60	0	1
4.52-5.08	24	13	10.60-11.15	1	2
5.08-5.63	17	17	11.15-11.70	0	1
5.63-6.18	16	19	12.25-12.80	3	0
6.18-6.73	11	13	13.36-13.91	1	1
6.73-7.28	14	9	14.46-15.01	1	2
7.28-7.84	9	11	16.12-16.67	1	0
7.84-8.39	8	6			
Total number of blisters per photo				150	144

[a]Magnification factors: Photomicrograph number 1=4300X
Photomicrograph number 3=4300X

Table A24. Raw blister diameter measurements from photomicrograph numbers 4 and 5 for sample V-13

Measured blister diameter range[a] (mm)	Number of blisters in each diameter range		Measured blister diameter range[a] (mm)	Number of blisters in each diameter range	
	Photo 4	Photo 5		Photo 4	Photo 5
2.32-2.87	0	1	7.84-8.39	0	8
2.87-3.42	12	4	8.39-8.94	2	2
3.42-3.97	32	12	8.94-9.49	0	1
3.97-4.52	28	16	9.49-10.04	1	2
4.52-5.08	33	20	10.04-10.60	0	2
5.08-5.63	35	22	10.60-11.15	0	1
5.63-6.18	24	18	11.15-11.70	0	2
6.18-6.73	24	17	11.70-12.25	0	1
6.73-7.28	10	15	16.12-16.67	0	1
7.28-7.84	7	11			
Total number of blisters per photo				212	157

[a]Magnification factors: Photomicrograph number 4=4300X
Photomicrograph number 5=4300X.

Table A25. Raw blister diameter measurements from photomicrograph numbers 7 and 8 for sample V-13

Measured blister diameter range[a] (mm)	Number of blisters in each diameter range		Measured blister diameter range[a] (mm)	Number of blisters in each diameter range	
	Photo 7	Photo 8		Photo 7	Photo 8
1.76-2.32	1	1	6.73-7.28	11	14
2.32-2.87	0	2	7.28-7.84	6	9
2.87-3.42	2	8	7.84-8.39	11	4
3.42-3.97	10	9	8.39-8.94	6	5
3.97-4.52	8	23	8.94-9.49	1	0
4.52-5.08	15	24	9.49-10.04	0	2
5.08-5.63	18	22	10.60-11.15	2	0
5.63-6.18	18	19	11.15-11.70	1	0
6.18-6.73	15	24	13.36-13.91	1	0
Total number of blisters per photo				126	166

[a]Magnification factors: Photomicrograph number 7=4300X
Photomicrograph number 8=4300X.

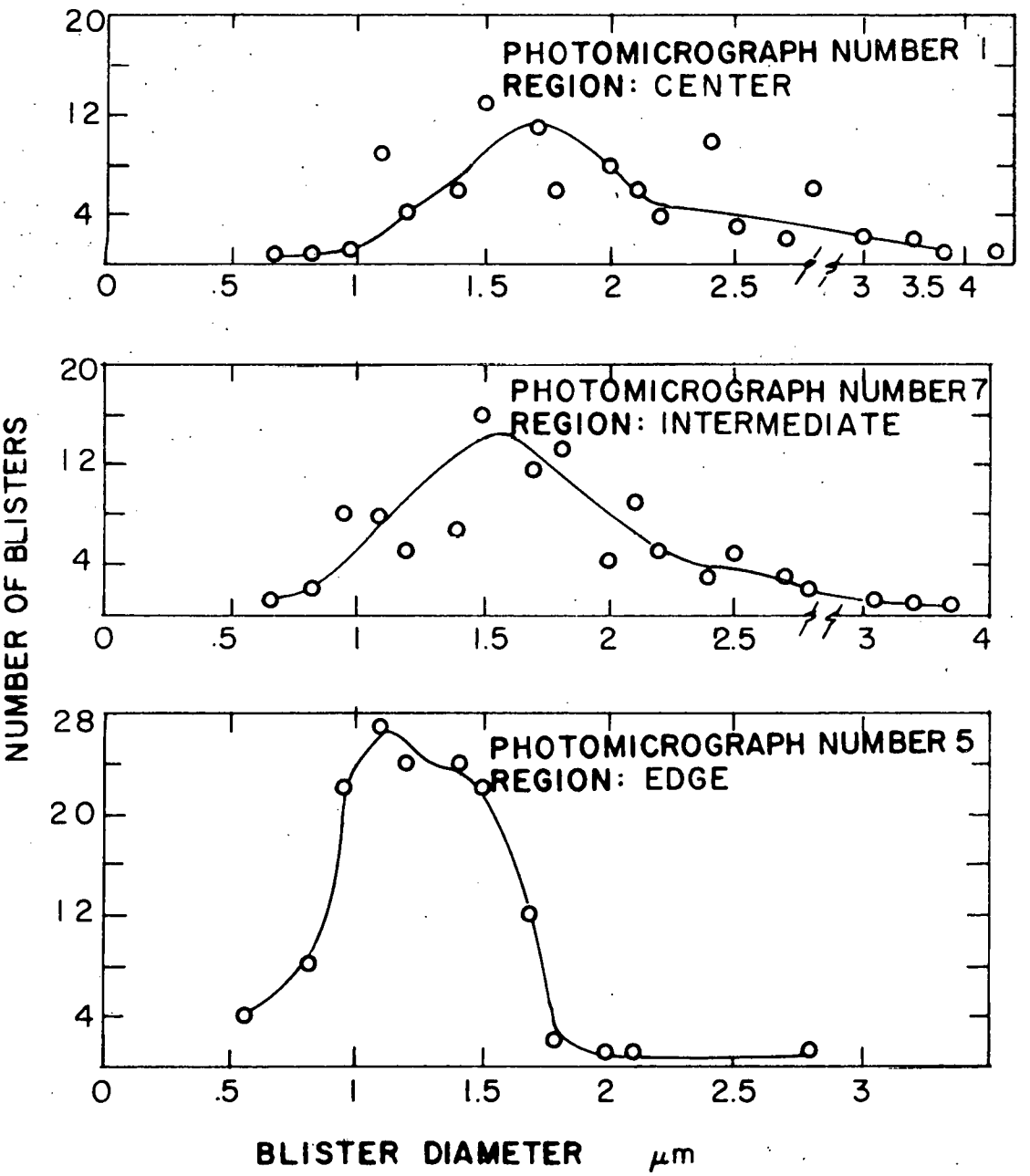

Figure A1. Blister size distribution plots for three photomicrographs of sample V-6 representative of the beam spot regions, center, intermediate and edge

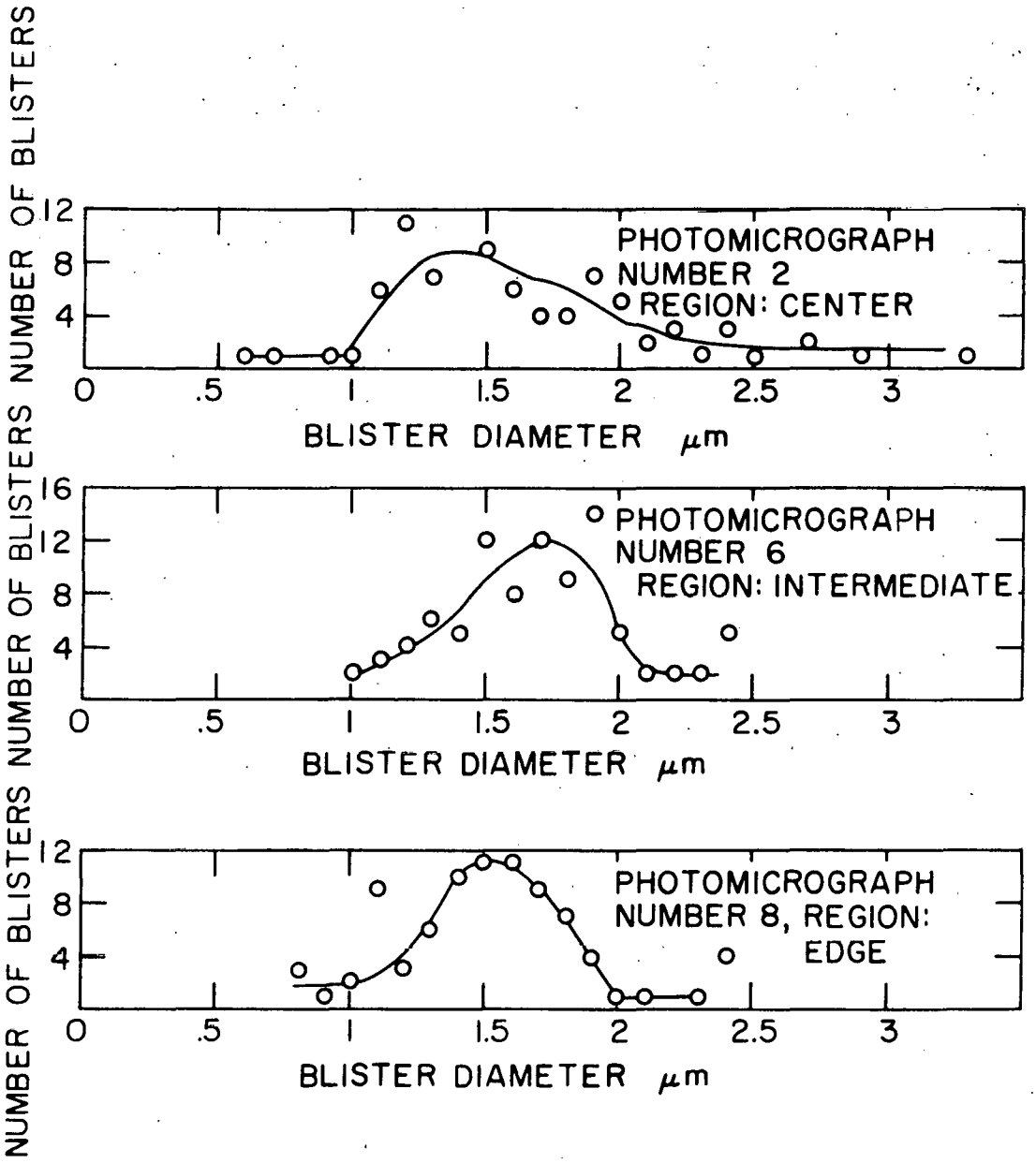

Figure A2. Blister size distribution plots for three photomicrographs of sample V-7 representative of the beam spot regions, center, intermediate and edge

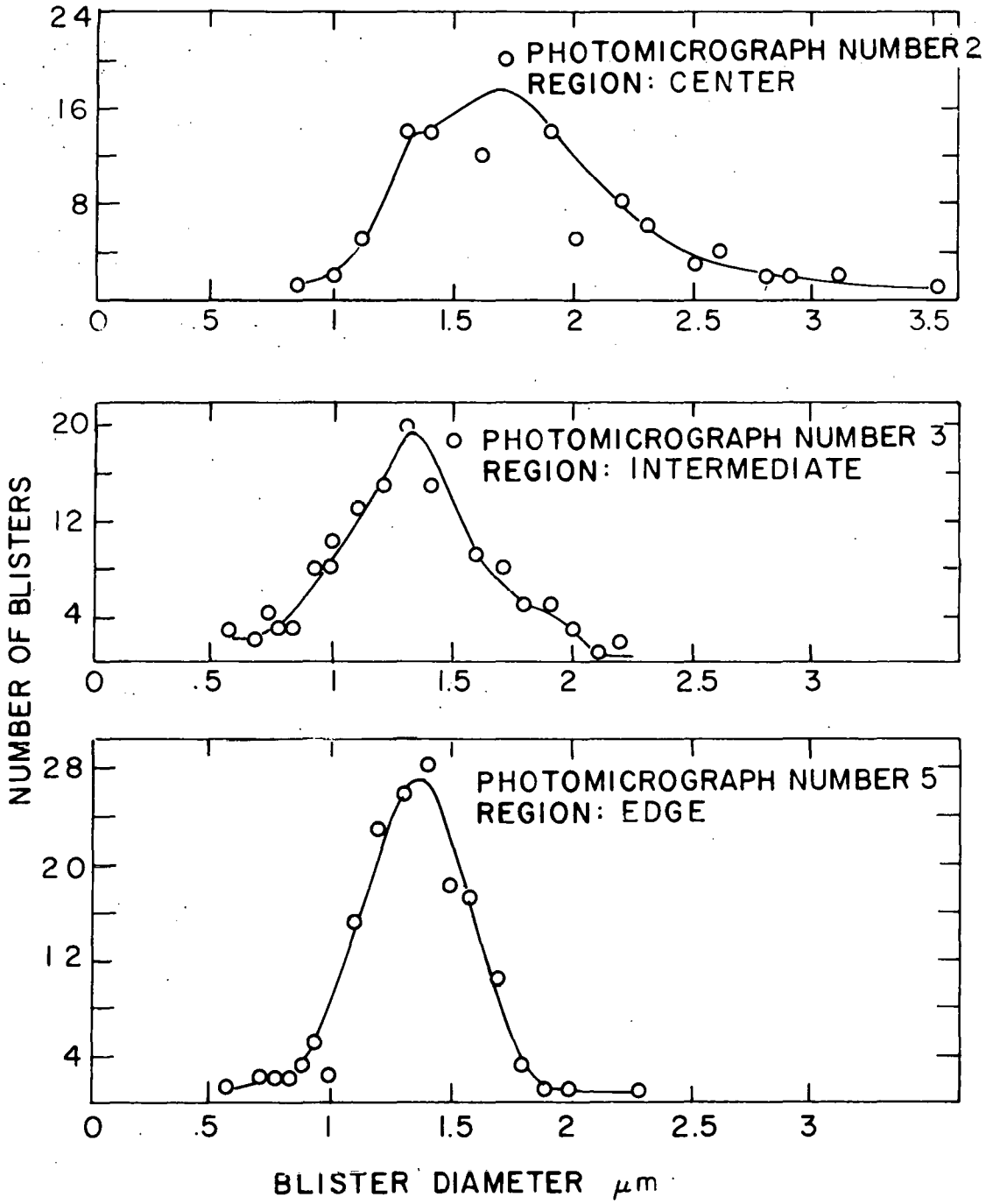

Figure A3. Blister size distribution plots of three photomicrographs for sample V-8 representative of the beam spot regions, center, intermediate and edge

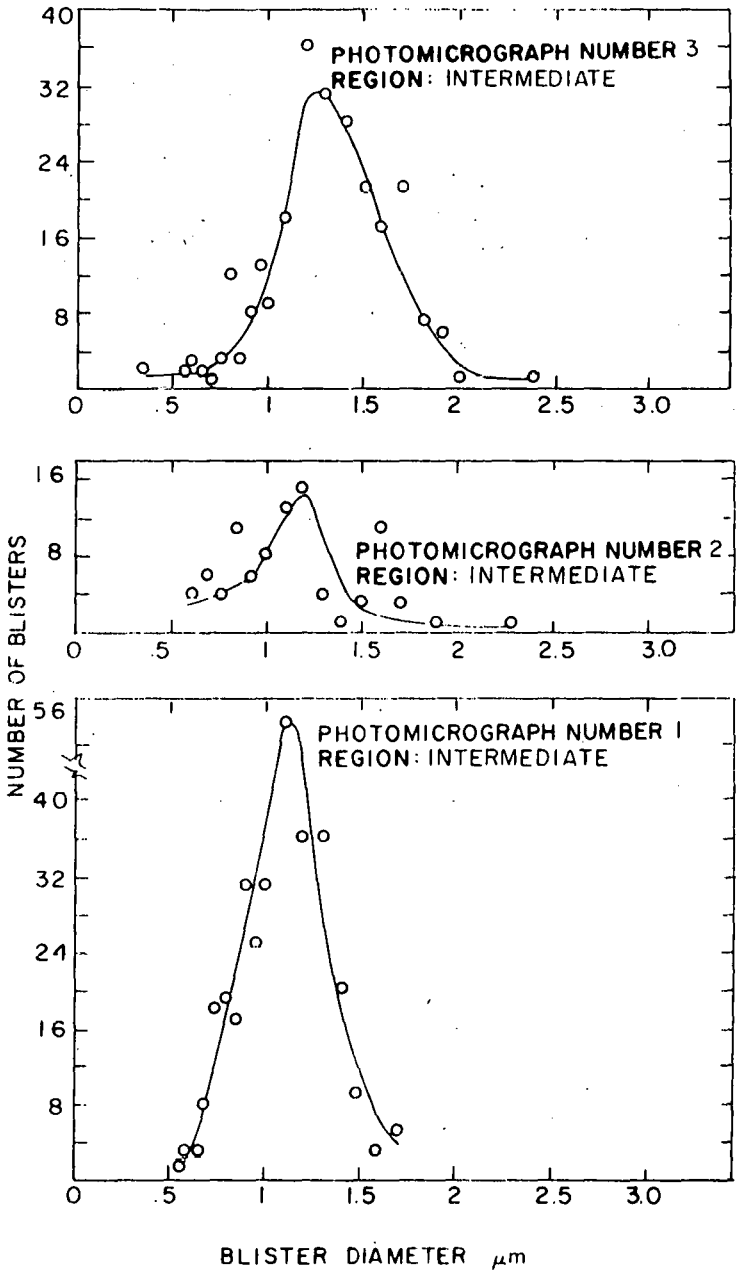

Figure A4. Blister size distribution plots for three photomicrographs of sample Y-9 representative of the beam spot intermediate region

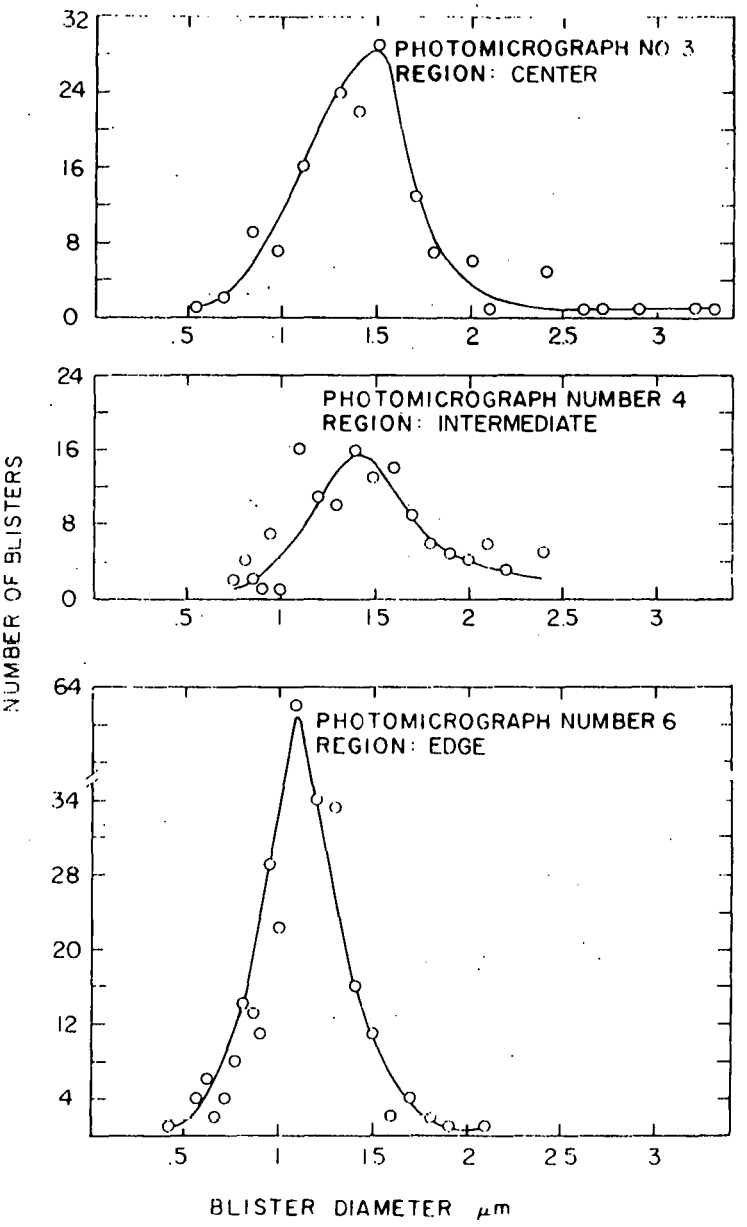

Figure A5. Blister size distribution plots for three photomicrographs of sample V-10 representative of the beam spot regions, center, intermediate and edge

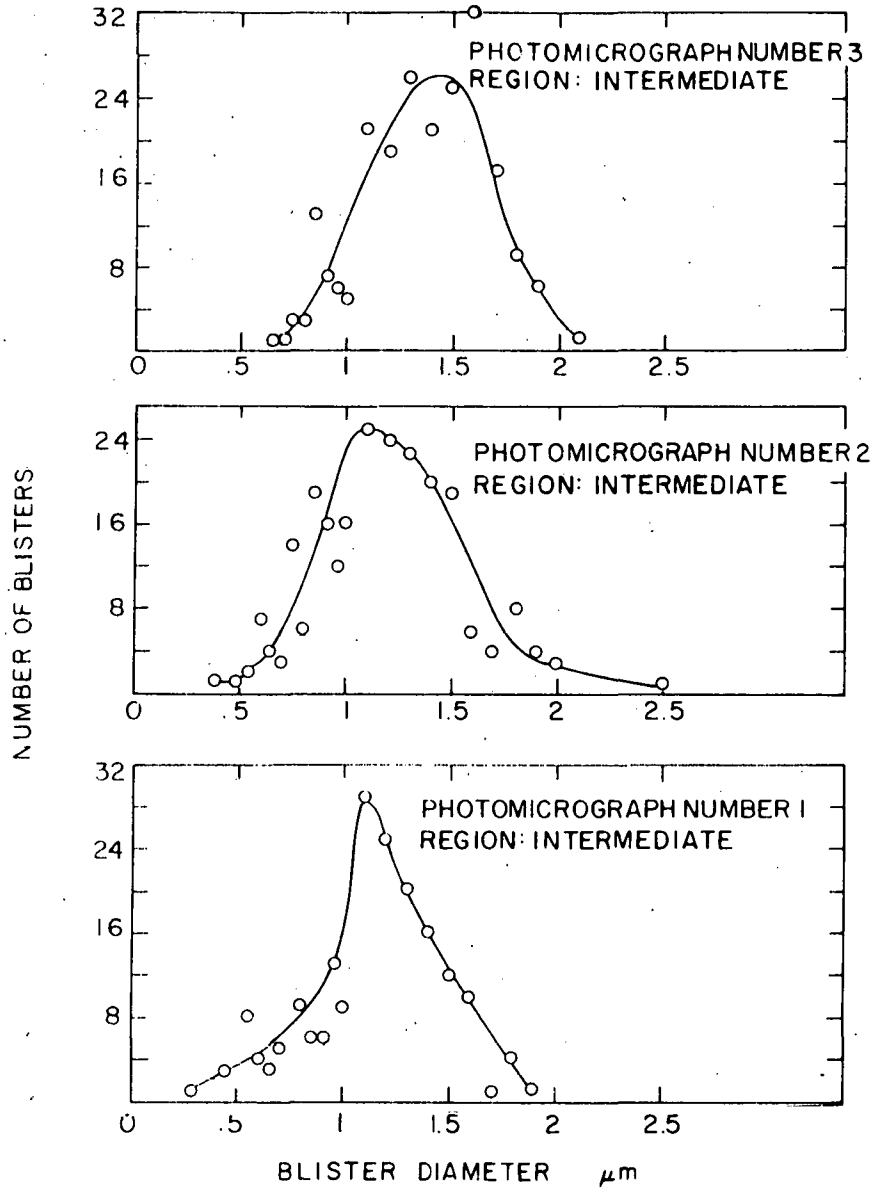

Figure A6. Blister size distribution plots for three photomicrographs of sample Y-11 representative of the beam spot intermediate region

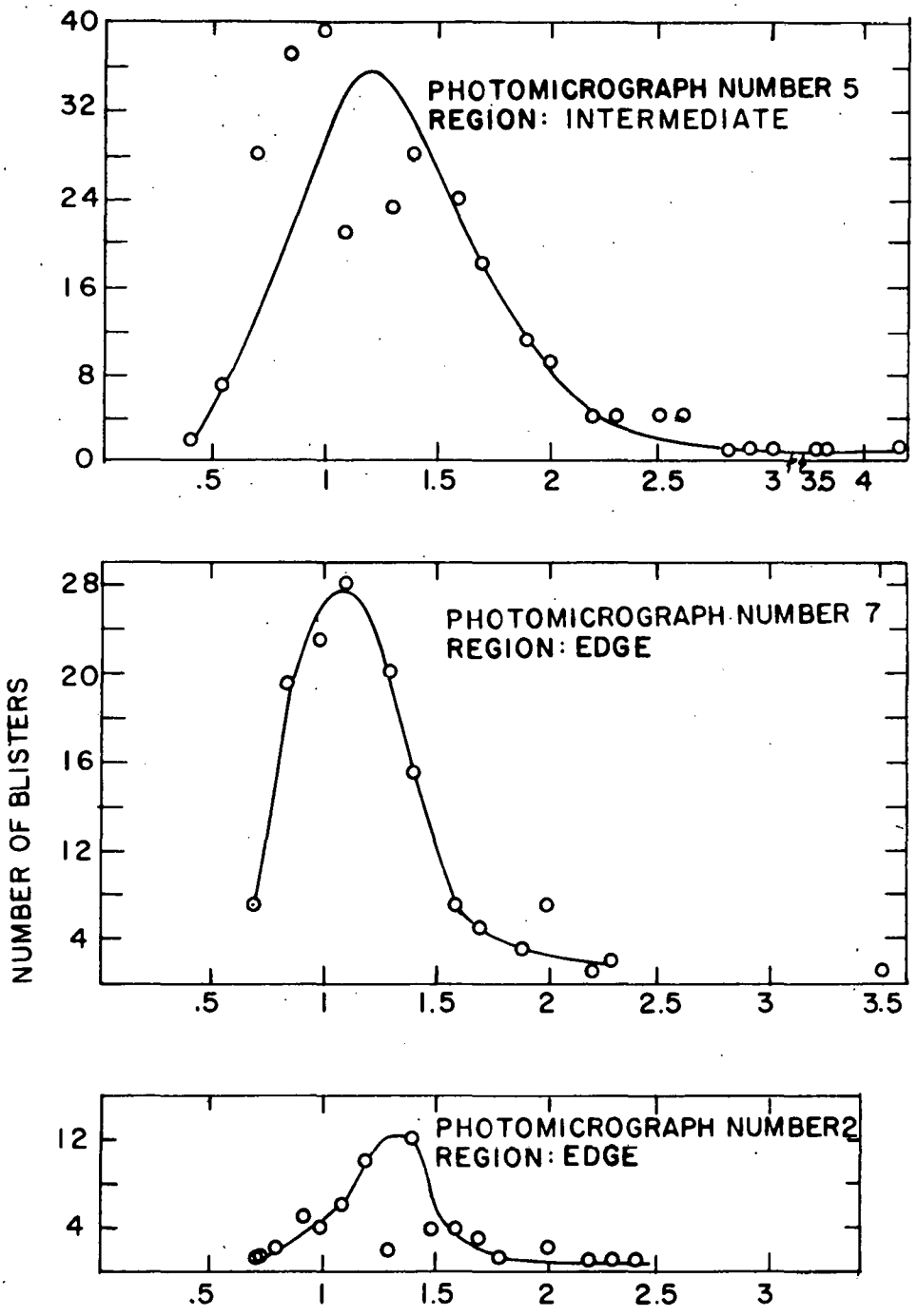

Figure A7. Blister size distribution plots for three photomicrographs of sample Y-12 representative of the beam spot regions, intermediate and edge

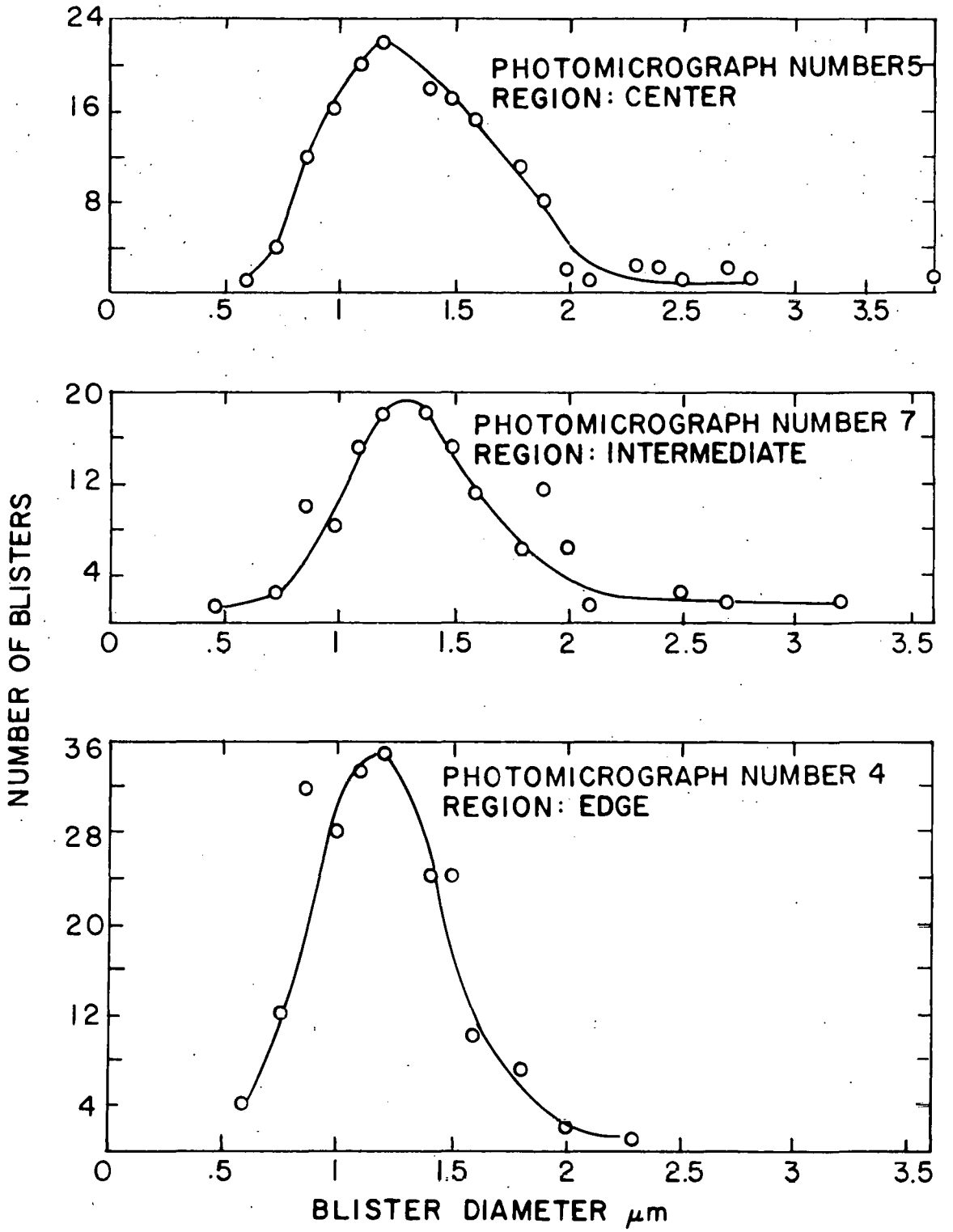

Figure A8. Blister size distribution plots for three photomicrographs of sample Y-13 representative of the beam spot regions, center, intermediate and edge

IX. APPENDIX B

This appendix contains the results of interstitial analyses performed on irradiated and unirradiated portions of the samples used in this research. The gas analyses were carried out using vacuum fusion techniques while carbon analyses were made using the combustion method. The irradiated portions of the samples were obtained from the center of the beam spot region and included most of the beam spot area. The unirradiated portions of the samples were obtained from a region shielded from the proton flux near the edge of the sample disc.

Table B1. Interstitial analysis results for the individual samples

Sample number	Analysis results for the unirradiated material by weight (ppm)				Analysis results for the irradiated material by weight (ppm)		
	C	H	O	N	H	O	N
V-1	44	9	120	8	11	145	26
V-2	49	4	113	3	1	105	---
V-3	43	10	128	3	3	64	5
V-5	151	12	300	98	11	305	125
V-6	179	11	275	100	12	345	130
V-7	154	2	220	98	10	370	130
V-8	154	<1	260	92	4	344	120
V-9	132	2	215	100	9	295	130
V-10	131	12	245	110	14	350	135
V-11	142	11	210	110	11	350	140
V-12	186	7	275	115	9	265	135
V-13	194	6	310	130	22	480	140
Nb-1	12	3	400	44	9	500	70
Mo-2	<5	--	45	---	--	---	---